PREPARATION AND EVALUATION OF MOLECULAR IMAGING PROBES
FOR BREAST CANCER

By

Mahmoud Mohamed El-Gamal, B.Sc.

A Thesis

Submitted to the School of Graduate Studies

In Partial Fulfillment of the Requirements

For the Degree

Master of Science

McMaster University

MASTER OF SCIENCE (2014) McMaster University

(Chemistry and Chemical Biology Department) Hamilton, Ontario

TITLE: PREPARATION AND EVALUATION OF MOLECULAR IMAGING PROBES FOR BREAST CANCER

AUTHOR: Mahmoud Mohamed El-Gamal, B.Sc. Honors (German University in Cairo)

SUPERVISOR: Professor John F. Valliant

NUMBER OF PAGES: xiii, 76

Abstract

Breast cancer remains the most commonly diagnosed cancer among women over the age of 20, as recently reported by the Canadian Cancer Society. Studies have shown a strong correlation between early detection and increased survival rates thus it is important to have a means to adequately screen and detect breast cancer. Currently, tests are limited to traditional imaging methods such as ultrasound (US), magnetic resonance imaging (MRI) and standard mammography. There remains a need for a molecular imaging probe that is capable of providing further prognostic information particularly with respect to assessing tumour aggressiveness and the likelihood of a cancer to metastasize.

Overexpression of the insulin receptor (IR) has been detailed in patients with breast cancer but there is currently no means of non-invasive and quantifiable detection of the receptor. The goal of the work described here was to prepare an insulin derived nuclear imaging probe via direct coupling of a prosthetic group bearing a radionuclide to the B29 lysine (B29-Lys) residue of the hormone. Benzoic acid bearing halogens were chosen as model compounds. The lead candidate N-[4-fluorobenzoyl]-(B29-Lys) insulin (**4**) was prepared in 60% overall yield and showed affinity for the IR similar to that of native insulin (IC$_{50}$=3.6 nM). The ^{18}F analogue (**9**) was successfully synthesized and showed high stability (up to 4 hours) post formulation in both saline and phosphate buffered solution (PBS).The product represents a promising new probe for assessing the role of the IR in cancer growth and metastasis.

A complementary strategy for imaging markers of tumour aggressiveness was investigated through the development of a novel ultrasound probe. A pretargeting approach involving urokinase plasminogen activator receptor (uPAR), which is known to play a role in cancer metastasis, was used to develop the agent of interest. Here, an *in vivo* reaction between

tetrazine tagged microbubbles (MBs) and anti-uPAR antibodies conjugated to trans-cyclooctene (TCO) was employed. Following preparation of the antibody conjugate and tetrazine functionalized MBs, preliminary *in vitro* testing in a flow cell system was conducted. Results showed the ability of the uPAR expressing cells to exclusively capture the tetrazine MBs after they have been previously incubated with the TCO anti-uPAR antibody. No capture was observed when the target and/or the antibody were absent. The contrast agent developed represents the first MB targeted against uPAR and has the potential to impact current diagnostic paradigms particularly given the widespread use of ultrasound in cancer patient management.

Acknowledgements

I would like to start by thanking my supervisor, Dr. John Valliant, for imparting his knowledge, wisdom and experience with me during my time with him. I appreciate the opportunity to work in such a high-level facility with access to cutting edge equipment. Your dedication to perfection and professionalism instills key concepts in us all that we will continue to carry through the rest of our lives. Your ability to bring forth innovative work and allow room for growth and expansion truly creates an environment to flourish in.

Also imperative in my success with this thesis were my additional two committee members – Dr. Alex Adronov and Dr. Paul Harrison. Your input and constructive criticism allowed me to delve further into my research and build a better base with which to move forward. Thank you for the time you put into my project and thesis and in helping me to become a better scientist.

I would like to thank all the members of the Valliant Research Group for their support, input and collaborations to my work. In particular, I would like to thank Dong Hyun Kim for passing on the insulin torch and teaching me the core basics of radiochemistry. I would also like to give a special thanks to Megan Blacker for all of her help and support with my project, both in and out of the lab. I would also like to thank Kirk Green in the mass spectrometry labs for all his help and my senior colleague Aimen Zlitni for his help in our collaborative work towards the end of my thesis.

I would like to give many thanks to my family, whom have always been an important support network and sounding board from which I can lean upon and grow. Thank you to my parents for leading by example by always being the most genuine, hardest-working people I know. Your hard work has allowed me to get to where I am today. Thank you to my brother

Ahmed for always making me laugh and teaching me to relax and live life. Special thanks to my other half, my twin Moustafa, for embarking on this journey with me and always being my second set of hands and eyes in life.

Of course my greatest thanks of all is to my wife (and lab colleague) who inspires me every day to get up and work a little bit harder to achieve something great. Your outlook on life allows me to be a better and stronger scientist, husband and man. And to our wonderful son Malik, your birth instilled in me a sense of drive and dedication I had never felt before. This thesis, and all of my future work, is for you.

Table of Contents

List of Figures

List of Schemes

List of Abbreviations and Symbols

2D	Two-Dimensional
3D	Three-Dimensional
Ab	Antibody
Akt	Protein Kinase B Pathway
ß	Beta
^{o}C	Degrees Celsius
ccDTPA	Cyclic Chelate Diethylene triamine penta-Acetic Acid
CD_2Cl_2	Deuterated Dichloromethane
CD_3CN	Deuterated Acetonitrile
CDI	Carbonyldiimidazole
CH_3CN	Acetonitrile
CI	Confidence Intervals
CNS	Central Nervous System
CPPs	Cell-Penetrating Peptides
csFBS	Charcoal Stripped Fetal Bovine Serum
CT	Computed Tomography
Cu	Copper
Cy5.5	Cyanine Dye
DBI	A1-Gly, B29-Lys-Di(Tert-Butyloxycarbonyl) Insulin
DCC	N,N'-Dicyclohexylcarbodiimide
DCM	Dichloromethane
DMF	Dimethylformamide
DMMA	Dimethylmaleic Anhydride
DMSO	Dimethyl Sulfoxide
DOTA	1,4,7,10-Tetraazacyclododecane-1,4,7,10-Tetraacetic Acid
dTE	Differential Targeted Enhancement
DTT	Dithiothreitol
ECM	Extra Cellular Matrix
EDC	1-Ethyl-3-*[3*-Dimethylaminopropyl*]*Carbodiimide
EI-MS	Electron Ionization Mass Spectrometry
ERK	Extracellular-Signal-Regulated Kinase
ESI-MS	Electrospray Ionization Mass Spectrometry
ES+	Electrospray Positive Ionization
F	Fluorine
fpVCT	Flat-Panel Volume Computed Tomography
Ga	Gallium
Gly	Glycine
HCC	Hepatocellular Carcinoma
HCl	Hydrochloric Acid
HIFU	High-Intensity Focused Ultrasound
^{1}H NMR	Proton Nuclear Magnetic Resonance Spectroscopy
HPLC	High Performance Liquid Chromatography
IC_{50}	Median Inhibition Concentration

IDE	Insulin Degrading Enzyme
ID/g	Injected Dose Per Gram
IGF-1	Insulin-Like Growth Factor-1
IGF-1R	Insulin-Like Growth Factor-1 Receptor
IgG_{2a}	Immunoglobulin G_{2a} Subclass
^{111}In	Indium-111
I	Iodine
IR	Insulin Receptor
I.U.	Injected Unit
K_2CO_3	Potassium Carbonate
kDA	Kilo Daltons
λ	Lambda
LCMS	Liquid Chromatography Mass Spectrometry
Ly-6	Lymphocyte Antigen 6
Lys	Lysine
MALDI-TOFMS	Matrix Assisted Laser Desorption Time of Flight Mass Spectromety
MAP	Mitogen Activated Protein
MB_C	Control Microbubbles
MBq	Mega Becquerel
MBs	Microbubbles
MB_{Tz}	Tetrazine Microbubbles
MB_{uPAR}	Microbubbles tagged with Anti-uPAR Antibodies
MB_V	VEGFR2-targeted Microbubbles
mCi	Millicurie
MeOTf	Methyl Triflate
MHz	Mega Hertz
MI	Molecular Imaging
μCi	Microcurie
min	Minute
MMPs	Meta-Metallo-Proteinases
MRI	Magnetic Resonance Imaging
m/z	Mass to Charge Ratio
Na_2HCO_3	Sodium Bicarbonate
NaOH	Sodium Hydroxide
NHS	N-Hydroxysuccinimide
N_2	Nitrogen Gas
NIRF	Near-Infrared Fluorescence
nm	Nanometer
nM	Nanomolar
N	Normal
PBS	Phosphate Buffer Saline
pCR	Pathologic Complete Response
PET	Positron Emission Tomography
Phe	Phenylalanine
PI3K	Phosphotidylinsositol 3-Kinase

ppm	Parts Per Million
Re	Rhenium
SPECT	Single Photon Emission Computed Tomography
$t_{1/2}$	Half-Life
TBAOH	Tetrabutylammonium Hydroxide
^{99m}Tc	Technetium-99 Metastable
TCO	Trans-Cyclooctene
TEA	Triethylamine
TFA	Trifluoroacetic Acid
TFP	Tetrafluorophenol
t_R	Retention Time
TSTU	O-(N-Succinimidyl)-*N,N,N',N'*-Tetramethyluronium tetrafluoroborate
Tyr	Tyrosine
Tz	Tetrazine
uPA	Urokinase-Type Plasminogen Activator
uPAR	Urokinase-Type Plasminogen Activator Receptor
US	Ultrasound
UV	Ultraviolet
VEGFR2	Vascular Endothelial Growth Factor Receptor 2

CHAPTER ONE: INTRODUCTION

1.1.Breast Cancer

According to the latest statistics published by the Canadian Cancer Society, breast cancer remains the most commonly diagnosed cancer in woman over the age of 20.[1] Additionally, breast cancer has a very high mortality rate in women, second only to lung cancer. It is true that the rate of mortality due to breast cancer has decreased in the past decade, but physicians are always faced with challenges in choosing the proper course of treatment and predicting treatment outcomes. One reason for such challenges is attributed to difficulty in designing efficient means for early detection, diagnosis, staging and evaluation of the metastatic potential and aggressiveness of the cancer.[2]

1.2.Detection of breast cancer

Currently, patients presenting with potential breast cancer go through a multi-step sequence of testing before arriving at a final diagnosis. In most cases, patients will undergo a series of tests including US, standard mammography, MRI and eventually, US-guided biopsy. Studies have shown significant correlation between early detection and increased survival rates[3], which has led to a concerted effort by physicians and general health practitioners to focus on early detection and prevention.[4]

Although standard mammography is considered the "go-to" diagnostic method for most breast cases, its limitations are becoming increasingly apparent.[5] For example, a comparison between a regular mammogram of an invasive ductal carcinoma and a molecular imaging scan using a breast specific camera and the probe ^{99m}Tc-Sestamibi revealed a 10 mm lesion that went undetected by regular mammography (Figure 1).[6]

Mammography also does not provide information about metastatic potential which can be derived from molecular imaging technologies. As a result the discovery and validation of novel molecular imaging probes is an emerging area in cancer research.
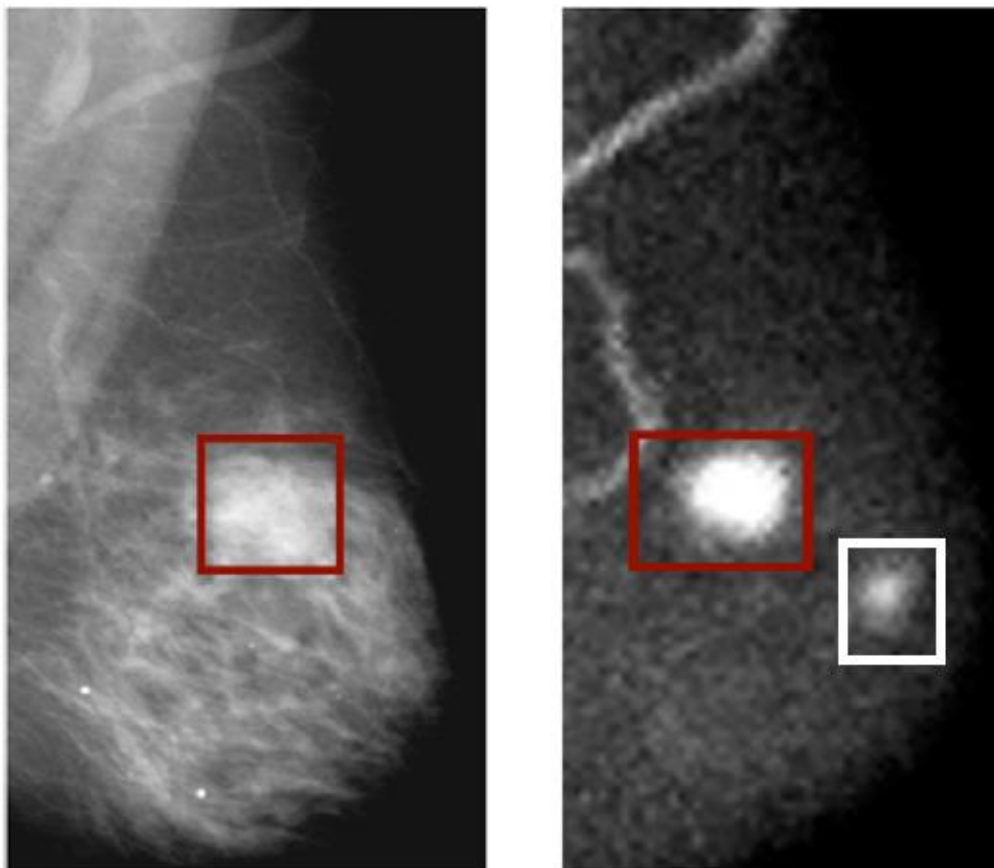
Figure 1 Regular mammogram (left) and molecular breast imaging scan using a [99mTc] tracer (right) of same patient. Cancer (red box) can be seen on both images, but only molecular breast image (using sestamibi) shows additional 10mm lesion (white box). (Reprinted with permission of [6])

1.3. Diabetes, obesity and breast cancer

The metabolic changes underlying diabetes, breast cancer and obesity were described as "parallel worlds" by Gary Taubes.[7] Although the epidemiology connecting the three diseases is very compelling, additional work and new *in vivo* imaging tools are needed to better understand the role of insulin and IR expression and dysregulaton.

Diabetes and obesity are two of the most prevalent conditions worldwide. In Canada alone, the number of individuals with diabetes in the general population will increase from approximately 1.4 million in 2000 to 2.4 million in 2016.[8] Additionally, approximately 90% of type-II diabetes is related to excess weight.[9] The metabolic environment in obese individuals is rich in free fatty acids along with other inflammatory mediators and cytokines.[10] The increase in those factors will lead to development of insulin resistance along with ß-cell dysfunction which can lead eventually to type-II diabetes.[10] Similarly, a connection between diabetes and cancer has been established. For instance, type-II diabetic patients treated with drugs that increase insulin release have higher risk and poor prognosis in many types of cancer including breast and prostate cancer.[11]

Clinical studies have also shown that diabetic breast cancer patients treated with metformin (a drug used for the treatment of type-II diabetes and its mechanism of action is via inhibition of gluconeogenesis without increasing insulin secretion) showed higher pathologic complete response (pCR) rates with neoadjuvant chemotherapy than did other diabetes medications.[12] When studying the connection between obesity and cancer Calle *et al.* found that cancer mortality is influenced by the presence of obesity.[13] It is believed that chronic excess energy intake causes obesity, which is a major predisposing factor to develop insulin resistance and hyperinsulinemia.[14] The latter is a common pathological condition in both obesity and type-II diabetes where the increase in circulating insulin levels and insulin/insulin-like growth factor-1 (IGF-1) along with the decrease in the latter binding protein activates systems known to play a key role in tumour development

including extracellular-signal-regulated kinase (ERK) and phosphotidylinsositol 3-kinase (PI3K) pathways.[14] There is a hypothesis that this insulin/insulin-like growth factor axis plays a fundamental role in connecting diabetes, cancer, and obesity.[7] A suitable imaging tool that can be used to non-invasively study this system in patients could bring about a paradigm shift in understanding the relationships between these conditions while also providing a tool for early detection and characterization of cancer.

1.4. Insulin

Insulin is a low molecular weight protein discovered in 1921 and is one of the most studied endogenous molecules due its key role in fundamental biochemical processes.[15] It consists of two peptide chains, A and B (Figure 2), connected by two disulfide bridges. The A-chain consists of 21 amino acids while the B-Chain has 30.[15] The main role is to ensure glucose homeostasis, however it is also involved in tissue growth due to its anabolic effect on muscles.[16] Elevated fasting blood glucose is indicative of diabetes which results from an insufficient secretion of pancreatic insulin (type I diabetes) or the inability of existing insulin to perform its function in lowering blood glucose levels (type II diabetes). Subcutaneous administration of insulin or derivatized forms is the most common treatment for diabetes.[15]

Apart from its key role in glucose homeostasis, insulin is known for its anabolic function stimulating cell growth and proliferation, especially in skeletal muscles.[16] This function can be accomplished directly via acting on the IR or indirectly via the insulin like growth factor(IGF) system.[17,18] The mechanism involves activation of receptor

tyrosine kinases via both insulin and IGF-1 activating their receptors; IR and IGF-1 receptor (IFG-1R), respectively. A hybrid IGF-1/IR exists which can be activated by insulin to stimulate specific IGF-IR signaling pathways.[17] Some of those are important oncogenic pathways like the mitogen-activated protein (MAP) kinase pathway and the phosphoinositol-3 kinase/Akt (PI3K-Akt) pathway which are known to play a role in progression towards cancer.[19] Whether the anabolic effect of insulin is due to inhibition of cell death or stimulation of cell growth is still being studied. A tool to understand the molecular mechanisms involved in insulin biochemistry would be of great utility in research in this field of study.
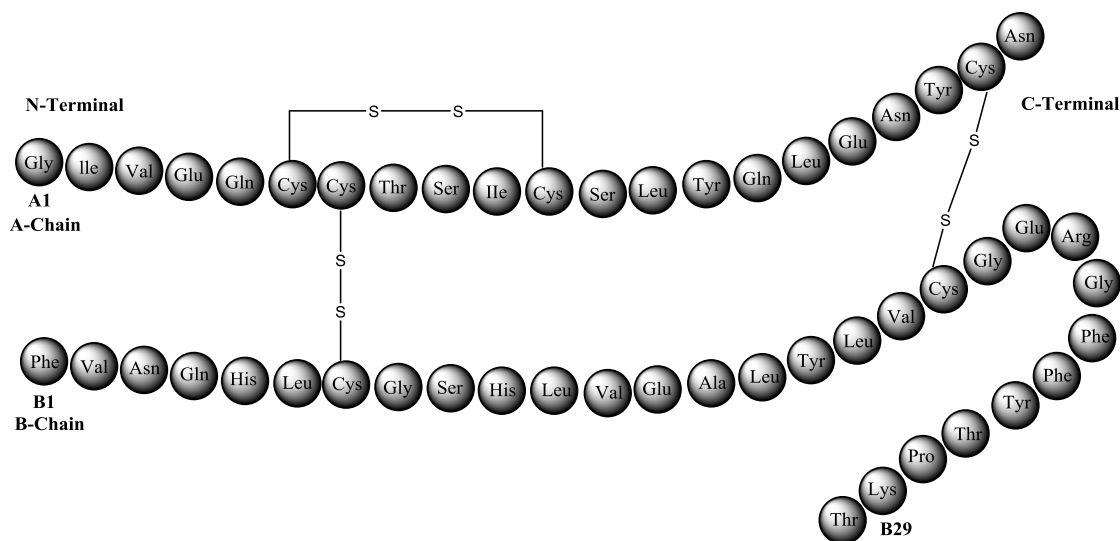
Figure 2 Schematic representation showing the amino acid sequence and disulfide bonds making up human insulin.

1.5. The IR in cancer

 IRs were found to be overexpressed in several tumours, including breast, colon, lung, ovary, and thyroid carcinomas.[20–23] In particular the IR-A isoform is the form that is overexpressed in many types of malignant cells.[23] This isoform was also found to bind

to IGF-2 and form hybrid IR/IGF-1 receptors.[23] IR content in human breast cancer was measured and noted to be 10 fold higher than that typically found in normal breast tissue.[24] A method to quantify the content of IR in cancer would be of great value, especially with the emergence of IGF-1R and/or IR-targeted therapies.[25,26] Strategies for targeted IGF-1R therapy include IGF-1R-targeted monoclonal antibodies, IGF mimetic peptides to inhibit ligand binding, low molecular weight molecules to inhibit its tyrosine kinase activity, and antisense aptamers.[27] Tyrosine kinase inhibitors are the most promising candidates and a number are currently in clinical trials.[28] For the monoclonal antibody inhibitors of IGF-1R clinical results have been underwhelming where one hypothesis is that compensatory mechanisms using the IR can be accessed by the tumour. As a result, tumours with low IR content respond better than those with high levels of IR.

1.6. Molecular imaging

Molecular Imaging (MI) is a tool that can be used to assess biochemical changes by visualizing interactions of a biological target with a molecular probe.[29] For example, for nuclear imaging, detectors that are sensitive to gamma rays are used to visualize the distribution of radiolabeled compounds. These methods include positron emission tomography (PET) and single photon emission tomography (SPECT)[30,31] which have the sensitivities needed to quantify changes in expression of specific receptors or the activity of enzymes and transporters. An emerging MI method is US imaging which utilizes non-ionizing radiation and targeted US bubbles as the contrast agent. A more extensive discussion of this particular technique can be found in chapter four.

1.7.Peptides in nuclear imaging

Peptides and proteins have been used extensively to develop new molecular imaging probes. One example of a peptide that has been used successfully in the clinic for detection of neuroendocrine tumours is ^{111}In-Octreotide, which resembles the peptide endocrine hormone somatostatin in its structure.[29,32] When selecting a peptide vector to create a MI probe it usually has a relatively small size (less than 50 amino acid residues), high binding affinity for the target (low-nanomolar range), high metabolic stability and the ability to achieve high target-to-nontarget ratios (specificity).[33] The advantages of using peptides are that they are not immunogenic, their production and development is relatively inexpensive, they typically show rapid plasma clearance due to renal excretion and are often internalized thereby facilitating retention at the target of interest.[33]

1.8.Insulin based nuclear imaging probes

Many attempts to radiolabel insulin have been reported in the literature. However, a significant number lacked complete characterization and/or validation. Most viable insulin-based constructs are derived from the parent hormone where the radioisotope is attached at a specific site so as to not perturb affinity or specificity. These are summarized here based on the isotope and prosthetic groups used.

The gold standard for studying insulin biochemistry *in vitro* is ^{125}I-insulin which is a product of direct iodination of insulin bearing the isotope at the A14 tyrosine (A14-Tyr) residue.[34] This probe is prepared using well-known lactoperoxidase or chloramine-T methods. By optimizing the pH and molar ratios of insulin and iodine it is possible to preferentially (but not exclusively) produce the A14-Tyrderivative which is stable and

bioactive compared to other iodinated derivatives (i.e. A19-Tyr). However, ^{125}I is not a suitable isotope for imaging human subjects because of its low energy emission and long half-life which limits the use of such probe to *in vitro* assays and quantitative biodistribution studies.[34,35]

Virgolini and coworkers reported a double tracer imaging strategy that involved the use of ^{99m}Tc-Galactosyl-Neoglyco albumin and ^{123}I-A14-Tyrinsulin as a tool to diagnose human hepatocellular carcinoma (HCC).[36] *In vitro* studies indicated that HCC express more than a thousand fold higher binding sites for the ^{123}I-A14-Tyr insulin than normal liver cells. Human SPECT studies showed that the tracer accumulated in HCC lesions and enabled facile differentiation of healthy and diseased tissue in a small trial. Studies involving ^{123}I-A14-Tyrinsulin in other forms of cancer or further use in HCC have not been reported. This is likely due to that fact that the preparation of the agent is complicated by low radiochemical yields and there is significant deiodination *in vivo*.

[124]I labeled insulin was prepared so that PET could be used to study insulin distribution and IR binding *in vivo*.[37] The [124]I insulin was prepared by direct electrophilic iodination at the A14-Tyr residue using cyclotron produced [124]I and chloramine-T as an oxidizing agent. The product was isolated by a complicated multi-step purification protocol and studies conducted in rats showed uptake in myocardium and liver tissue with very low uptake in the brain. The heart, liver and kidneys were visualized by PET after intravenous injection. However, there are challenges in the clinical use of this probe which included difficulty in separating unlabeled insulin from the formulation and

difficulty determining the exact specific activity at the time of formulation. Other attempts of labeling insulin with [124]I have been reported but they were low yielding and the labeled probe was not completely validated.[38] It is also important to note that [124]I is not an ideal radionuclide for imaging as the proportion of [124]I that decays by positron emission is low.[38]

An ^{111}In-labeled insulin based tracer was reported by Rowshanfarzad *et al.*[39] The labeling was achieved by conjugating insulin to the cyclic chelate diethylenetriamine pentaaceticacid dianhydride (ccDTPA) followed by treatment with [111]InCl$_3$. The radiolabeled complex was stable in human serum for at least 24 hours where no free ^{111}In or ^{111}In-DTPA was observed. Biodistribution studies in normal rat model were performed where uptake of the radiotracer showed high liver (24 hours post injection) and spleen uptake (24 hours post injection) (Figure 3) which was in agreement with the preclinical SPECT images (Figure 4). Complete biochemical validation for this tracer including its ability to bind the IR was not reported.
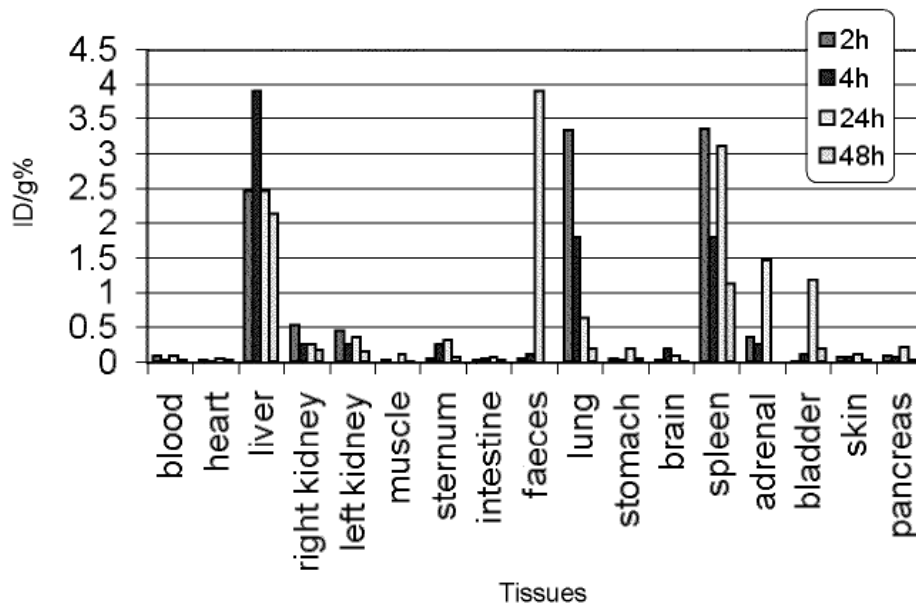
Figure 3 Biodistribution of ^{111}In-DTPA-insulin in normal rats at 2, 4, 24 and 48 hours post-injection. (Reprinted with permission of [39])
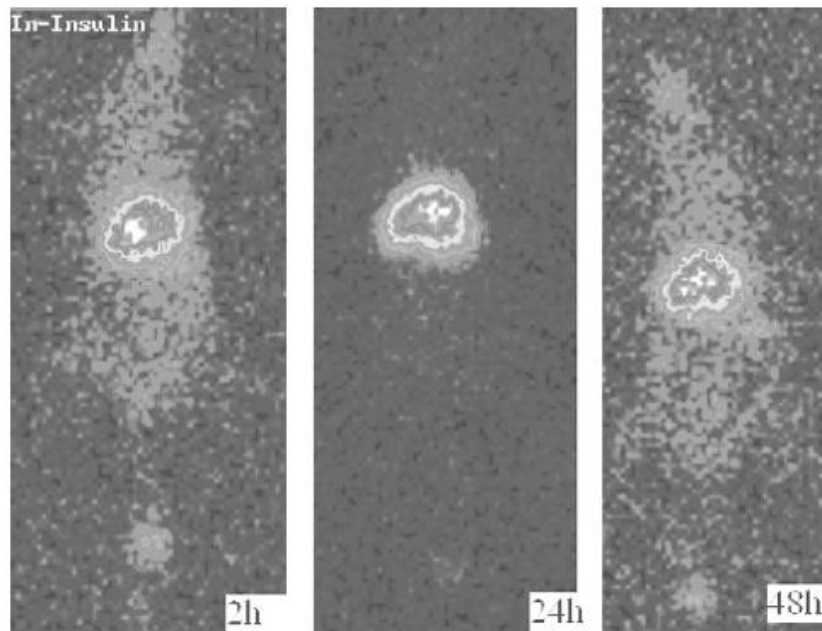
Figure 4 SPECT images of ^{111}In-DTPA-insulin in normal rats at 2, 24 and 48 hours post injection. The best image was acquired at 24 hours post-injection, as radioactivity was concentrated in the liver with minimal background signal. In the images for both the 2 and 48 hour time points, increased background signal is apparent due to uptake in the intestines. (Reprinted with permission of [39])

A related analogue, ^{67}Ga-insulin, was prepared from ^{67}Ga gallium chloride and the DTPA insulin derivative used to prepare the indium derivative.[40] The radiolabeled complex was stable in the mice serum for at least 24hours and biodistribution studies in normal rats showed high accumulation in the liver. Again however IR binding *in vitro* was not validated.

Kamei *et al.* studied the effect of cell-penetrating peptides (CPPs) on increasing the intestinal absorption of insulin via PET imaging of ^{68}Ga-1,4,7,10-tetraazacyclododecane N, N′, N″, N‴-tetraacetic acid insulin conjugates (^{68}Ga-DOTA-insulin).[41] Biodistribution studies in rats showed that CPPs co-administration significantly increased the ^{68}Ga-DOTA-insulin level in the liver, kidney, and circulation confirming their role in increasing the intestinal absorption of insulin. This is an example of how nuclear imaging can be used to support drug development.

[99m]Tc is an inexpensive isotope and it is the most widely used isotope in nuclear medicine. Direct labeling of insulin with ^{99m}Tc has been reported but was not effective because IR binding was affected and a mixture of radiolabeled products was formed. Another example is ^{99m}Tc labeled insulin that was designed as a tool to study the biochemistry and pharmacology of insulin *in vivo,* as reported by Sundararajan *et al.* [99m]Tc labeled analogues along with their non-radioactive rhenium (Re) surrogates were synthesized by linking a ^{99m}Tc chelate to the B1 phenylalanine (B1-Phe) position of a

protected insulin through a spacer group (Figure 5).[42] *In vitro* assays for IR binding of the Re analogues showed no difference from native insulin. These probes have been evaluated in a series of biodistribution and SPECT/CT studies in different preclinical disease models where the extent of specific and nonspecific binding was assessed and they are currently under further investigation in order to improve their pharmacokinetic profiles via means of structural modifications.
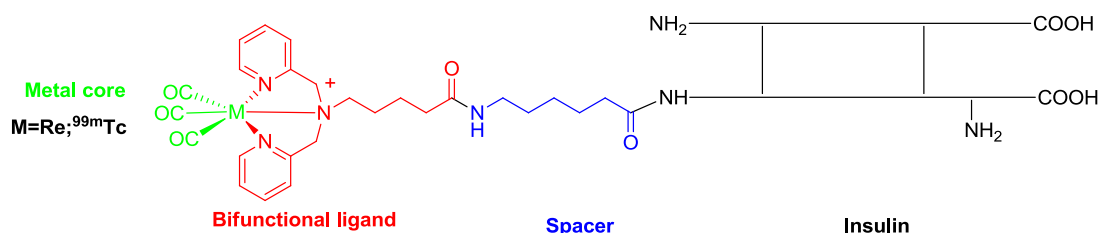
Figure 5 Human insulin and the target [99mTc/Re] insulin conjugates.[42]

[18]F-labeled insulin using a prosthetic group methodology designed for studying the IR *in vivo* using PET was initially reported by Shai *et al.* where a fluoromethylbenzoyl prosthetic group linked to a glycine (Gly) spacer attached to insulin at the B1 position binds human (IM-9) lymphoblastoid cells *in vitro* with an affinity for the receptor that is similar to that of native insulin.[43] Biodistribution studies and PET scans were performed in six rhesus monkeys where the tracer showed 95% stability and integrity for the first 5 minutes post injection which dropped down to 31% at 30 minutes post injection. The labeled tracer accumulated rapidly in the liver and unlabeled insulin blocked subsequent uptake by the liver. Both timing and reversibility of uptake and excretion of the analogue (using native insulin as a blocker) closely mimic the known

physiological processes by which insulin is cleared.[44] Unfortunately, both the chemistry and radiochemistry associated with preparing the probe were low yielding and involved extensive HPLC purification protocols which complicate clinical translation.

Another method for the preparation of ^{18}F labeled analogues of insulin via direct coupling of an active ester to the free amino of the B1-Phe position through a spacer group was developed in our research group. *In vitro* assays of the non-radioactive ^{19}F version showed similar binding to that of native insulin. The synthesis required a number of synthetic steps including protecting theA1-Gly and B29-Lysine (B29-Lys) positions of insulin. Protected insulin A1-Gly,B29-Lys-di(tert-butyloxycarbonyl) insulin (DBI) was synthesized to ensure site selective derivatization.[35] More recently, [18][F]N-fluorobenzoyl B1-Phe insulin was prepared using a novel emulsion labeling technology which greatly enhanced radiolabeling yields.[45] The product was tested for stability using mouse plasma and showed decomposition to a non-polar radioactive material. The percentage of decomposition from the compound based on analytical HPLC analysis was 50% at 30 min. Biodistribution in Female CD-1 nu/nu mice bearing CHO/HIRC tumours showed tumour uptake of $1.74 \pm 0.54\%$ injected dose per gram (ID/g) at 5 minutes and $0.3 \pm 0.1\%$ at 30 min post injection.[46] Clearance was predominantly via the renal system with some additional excretion via the hepatobiliary system (Figure 6).
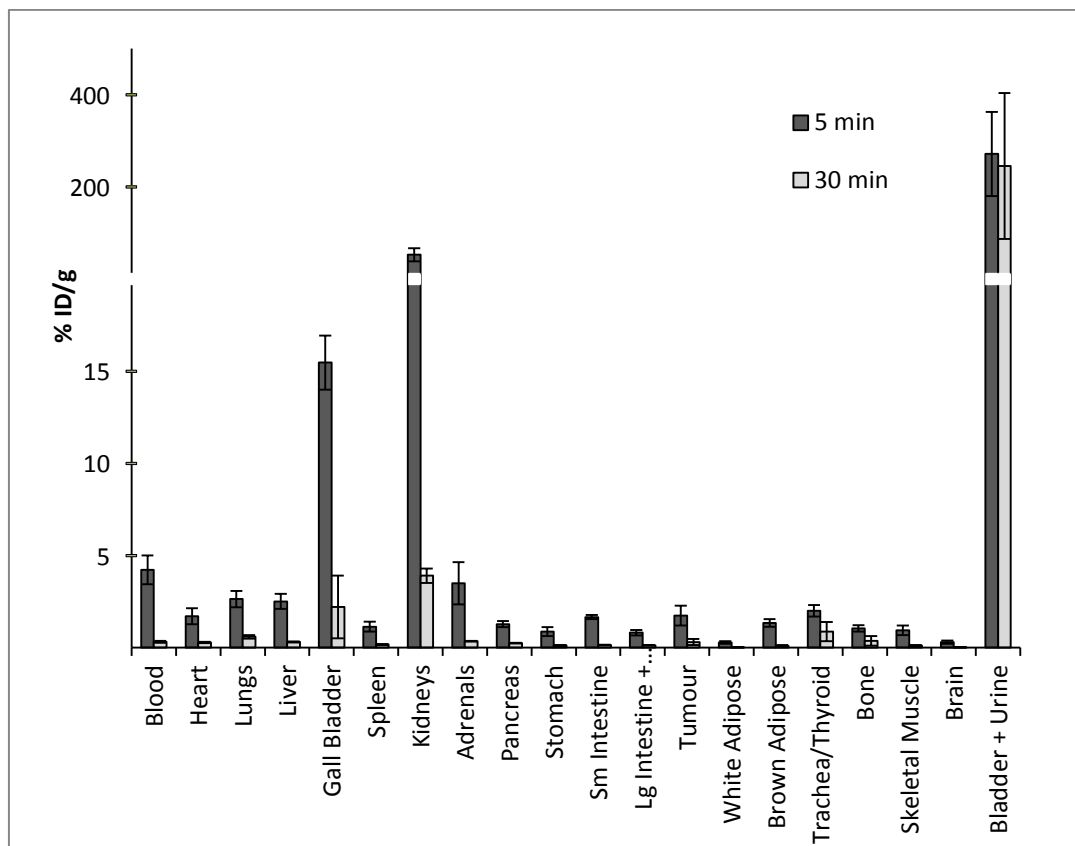
Figure 6 [18][F]N-fluorobenzoyl (B1-Phe) insulin biodistribution in female CD-1 nu/nu mice. (Reprinted with permission of [46])

1.9.B29-Lysderivatized insulin

Insulin has three primary and reactive amines where modification of the protein can potentially be carried out: A1-Gly, B1-Phe andB29-Lys residues. The crystal structure of insulin interacting with its receptor indicates that A1-Gly residue is involved in binding, consequently derivatization must be carried out at B1-Phe and B29-Lys residues.[15] Given the limitations of B1-Phe derived radiopharmaceuticals developed to date and considering the complex protecting group chemistry required to prepare compounds, B29-Lys is an attractive alternative. It has the advantage that it is highly reactive and can be selectively labeled by controlling the pH of the reaction medium.[47]

There have been a number of B29-Lys derivatives that have been reported, which are described here.

Aiming to extend the time of action of insulin; ^{3}H,N-palmitoyl B29-Lys insulin was prepared via direct coupling to the N-Hydroxysuccinimydyl ester of palmitic acid.[48] In a diabetic animal model, the duration of action was nearly twice that of unmodified human insulin, and the plasma half-life was nearly seven-fold that of the unmodified protein. Insulin action was longer and less variable than that of native insulin with improved pharmacokinetics. No data regarding IR receptor binding was reported although it was found that the derivative maintained its pharmacological potency.

Vitamin B12-[B29-Lys]derivatized insulin conjugate was prepared as a tool for oral delivery of insulin.[49] Carbonyldiimidazole (CDI) activated vitamin B12 was coupled to dimethylmaleic anhydride (DMMA) A1-Gly, B1-Phe di protected insulin and purified by ion exchange chromatography. It showed a significant glucose lowering effect maintaining the biological activity of insulin without interfering with IR recognition. A combination of molecular dynamics simulations and electron microscopy were used to assess the construct and indicated that chemical modification of insulin by linking a pendant group at the B29-Lys position does not interfere with IR recognition.[50]

Another example was based on transferrin conjugation at the B29-Lys of insulin. The derivative showed increased stability to enzymatic degradation when compared to native insulin. The degradation profiles of insulin, transferrin and the conjugate were evaluated in a solution containing trypsin based on HPLC analysis.[47] Many other

examples have been reported in the literature where modifying the B29-Lys of insulin had no effect on its biological activity, receptor recognition or stability.[48,51]

1.10. Hypothesis and objectives

The core hypothesis of the first component of the thesis is that derivatization of insulin at the B29-Lys position with a suitable radionuclide (e.g. [123]I or ^{18}F) and prosthetic group (Figure 7) will result in a MI probe that can be used to monitor changes in insulin biochemistry and IR expression *in vivo*. The desirable properties of a candidate probe are that it has high affinity for IR (IC_{50} close to or better than that of native insulin), stability *in vitro* (longer than the 5-10 minute plasma half-life of human insulin), ease of synthesis, blockable IR binding *in vivo* and high tumour uptake for IR expressing tumours.

In order to develop and refine the synthetic and HPLC methods, two simple N-succinimidyl active esters of benzoic acid were the initial targets. The specific choice of active esters was based on the fact that direct coupling to the B29-Lys position of insulin using other N-succinimidyl active esters has been previously reported.[41,51,52] Also, in our group the same benzoic acid ester has been coupled to the B1-Phe of insulin without affecting it's biological activity or IR binding.[35] Furthermore, the preparation of the ^{18}F and ^{125}I derivatives of the active esters of benzoic acid have been reported and they can be isolated in good yields.[53–55] Once the lead compounds were prepared and screened coupling to other prosthetic groups including those with a pharmacokinetic modifying linker were investigated which is described in chapter three.
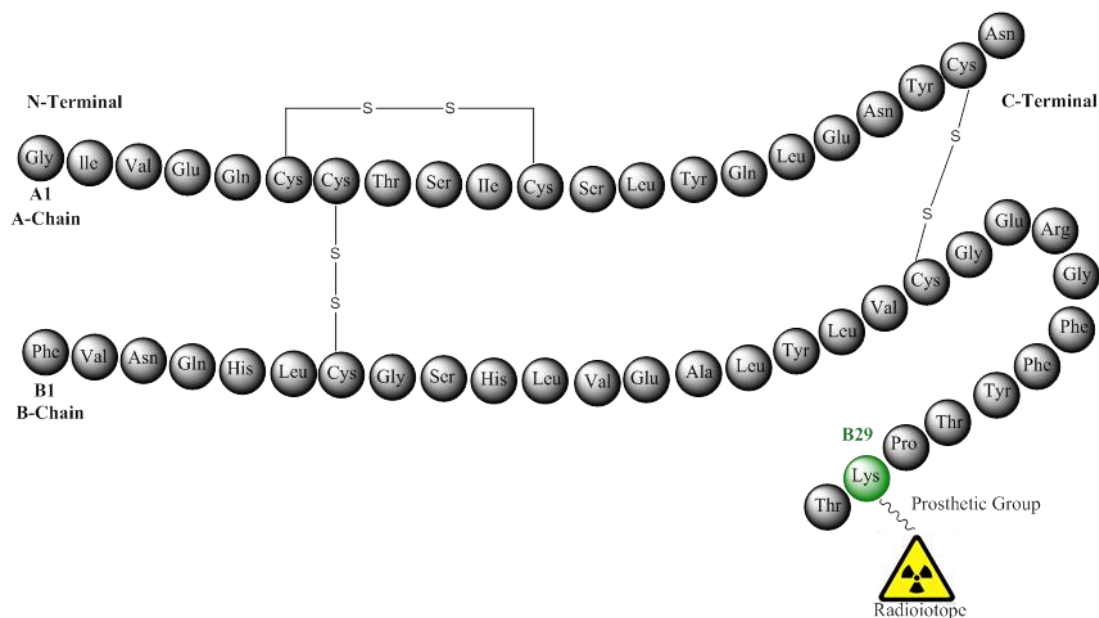
Figure 7 Schematic representation of the general target: a B29-Lysradiolabeled insulin derivative.

Subsequent to the work on insulin, a strategy was developed to enable US imaging to be used to visualize uPAR, which as mentioned previously, is a protein that is upregulated in breast cancer. The strategy utilizes a novel targeting methodology and gas filled MBs which act as US contrast agents. Details on the rationale and synthetic strategies which include the use of some novel bioorthogonal chemistry are provided in chapter four.

CHAPTER TWO: SYNTHESIS, PURIFICATION, CHARACTRIZATION, and *IN VITRO* SCREENING of B29-Lys DERIVATIZED INSULIN

2.1. Synthesis of N-succinimidyl benzoic acid active esters

As described in chapter one, the choice of simple halogenated benzoic acid active esters for the bioconjugation reaction was based on the fact that they are easy to synthesize, have been previously conjugated to insulin at different positions and methods to produce the radioactive analogues have been reported in the literature. Using a relatively simple synthetic procedure, 4-iodobenzoicacid was converted to its N-succinimidyl active ester by heating it with 1-ethyl-3-[3-dimethylaminopropyl]carbodiimide hydrochloride (EDC) and N-hydroxysuccinimide (NHS) in dry dimethylformamide (DMF) (Scheme 1). After 3 hours the product (**1**) was obtained as white crystalline solid in high yield (90%) following extraction. Proton nuclear magnetic resonance spectroscopy (^{1}H NMR) of the isolated product showed two key doublets corresponding to aromatic ring protons between 7.8 and 8.2 ppm and the remaining four methylene protons of the succinimide group were observed at 3 ppm (Figure 8). In a similar fashion; N-succinimidyl 4-fluorobenzoate (**2**) was synthesized according to the same procedure described above in 82% yield. ^{1}H NMR spectroscopy of the isolated product showed characteristic signals similar to those in (**1**) (Figure 9).
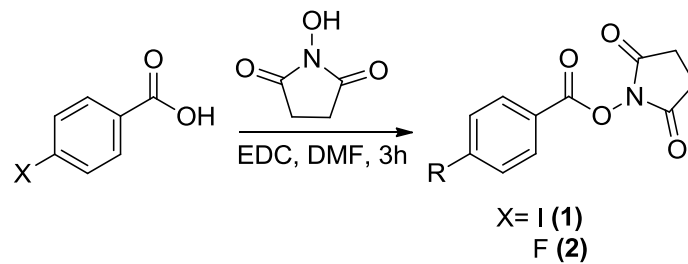
Scheme 1 Synthetic scheme for N-succinimidyl 4-iodobenzoate (**1**) and N-succinimidyl 4-fluorobenzoate (**2**).
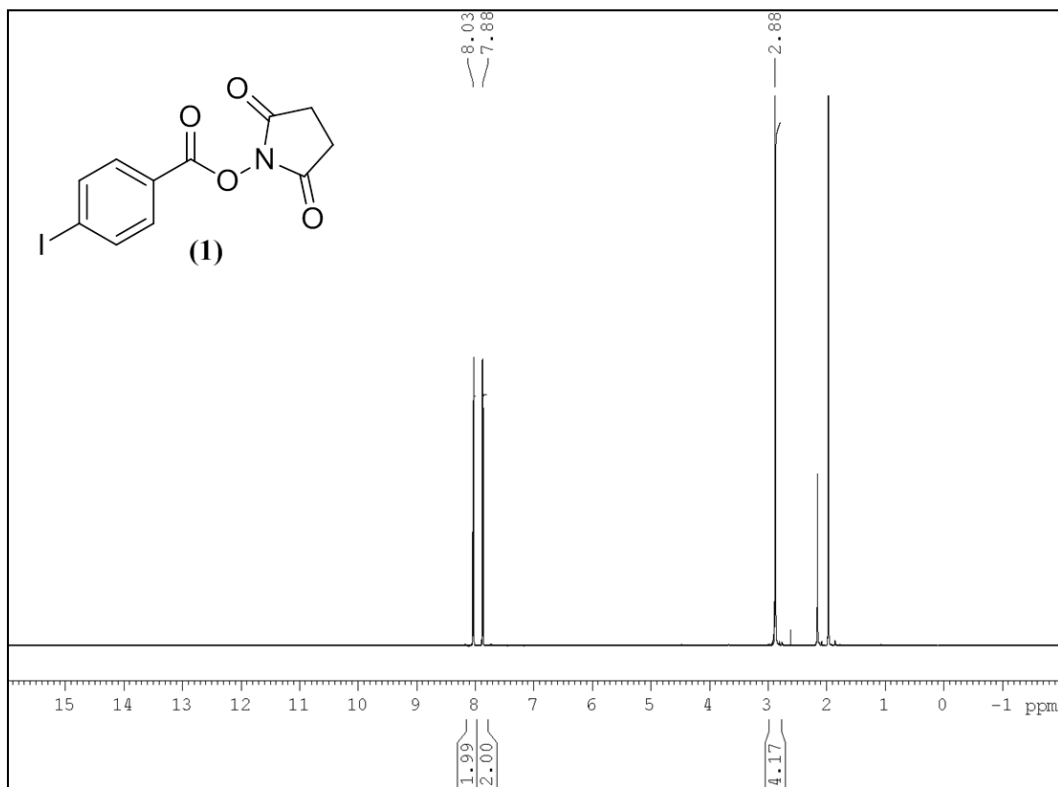
Figure 8 ^{1}H NMR (CD$_3$CN, 600.13 MHz) of N-succinimidyl 4-iodobenzoate (**1**), residual CH$_3$CN appeared at 1.94 ppm followed by a water peak at 2.1 ppm.
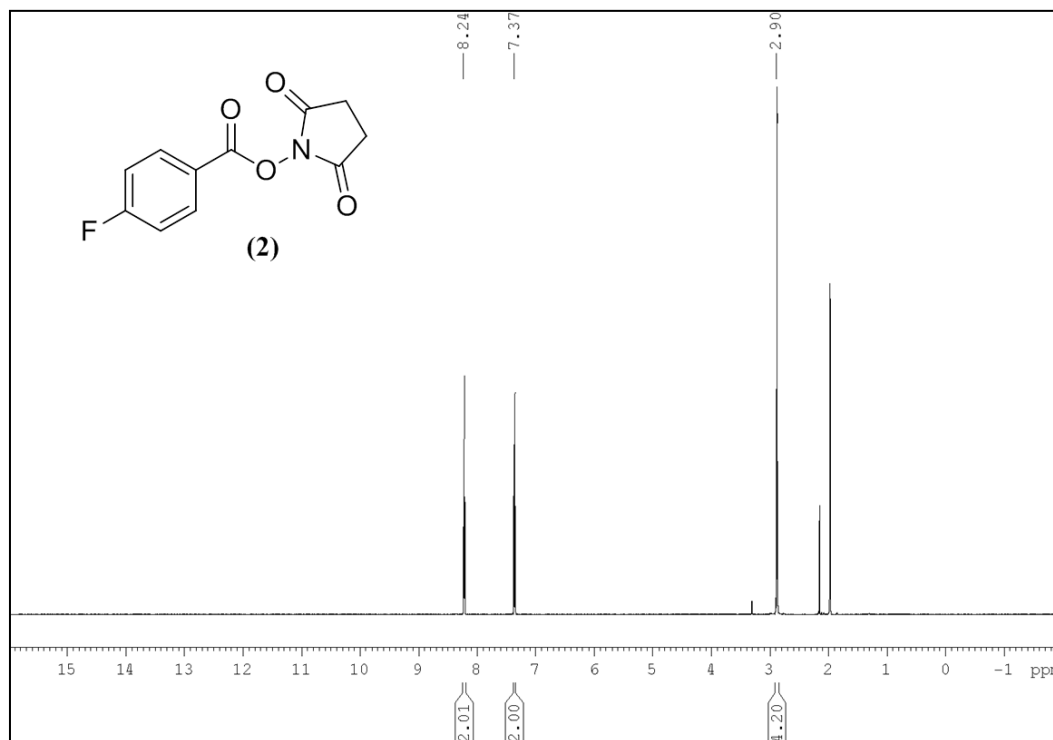
Figure 9 ^{1}H NMR (CD$_3$CN, 600.13 MHz) of N-succinimidyl 4-fluorobenzoate (**2**), residual CH$_3$CN appeared at 1.94 ppm followed by a water peak at 2.1 ppm.

2.2. Synthesis and purification of B29-Lys fluoro and iodo benzoic acid derivatized insulin

Different reaction conditions were investigated to find the best method for coupling the active ester to the B29-Lys of insulin. In parallel, an analytical HPLC method in order to separate different reaction products was developed where the optimal gradient was: Mobile phase A = (acetonitrile (CH$_3$CN) + 0.1 % trifluoroacetic acid (TFA)), Mobile phase B = (H$_2$O + 0.1 % TFA): Elution Conditions: 25% A to 100% A, 0 − 20 min; 100% to 75% A, 20 − 30 min; 75% A to 25% A, 30 − 32 min; 25% A to 100% A, 32 − 35 min. UV detection (λ = 240 nm) allowed for monitoring the reaction where t$_R$ for insulin was 9.3 min.

The reaction of insulin with N-succinimidyl 4-iodobenzoate was initially carried out in dimethylsulfoxide in 5% triethylamine (DMSO/TEA) at a pH of 10.5. Mass spectrometric analysis of the initial reaction showed peaks corresponding to di- and tri-substituted derivatives of insulin rather than the required mono-substituted one, which indicated that reaction conditions needed refining. To optimize the formation of the desired product, molar ratios were varied between 20:1 and 1:10 of the active ester and insulin, respectively, where the results showed that a ratio in the range of 1.5:1 gave the best results. Notably, a key step to enhancing selectivity involved dissolving insulin completely in basic medium before addition of the ester.

The ultimately successful conditions involved switching to a mixture of DMF and Borax buffer as the solvent using an insulin to active ester ratio of 1:1.5 at pH 9.5 (

Scheme 2). After 30 min at room temperature; N-[4-iodobenzoyl]-(B29-Lys) insulin (**3**) and N-[4-fluorobenzoyl]-(B29-Lys) insulin (**4**) were successfully synthesized as the predominant products. Purified materials were obtained by semi-preparative HPLC using a C18 column (**3**, Figure 10) and (**4**, Figure 11) and electrospray ionization mass-spectrometry (ESI-MS) indicated that the isolated insulin derivatives are monosubstituted where (**3**) showed a mass to charge ratio (m/z) of 6036 (Figure 12) and (**4**) showed a m/z ratio of 5930 (Figure 13), respectively.

Scheme 2 Synthesis of B29-Lys insulin derivatives (**3**) and (**4**).

Figure 10 Analytical HPLC chromatogram of crude reaction mixture (top) between insulin and (**1**).The bottom chromatogram shows the HPLC of purified (**3**). Elution Method: A = (CH$_3$CN + 0.1 % TFA), B = (H$_2$O +0.1 % TFA): Elution Conditions: 25% A to 100% A, 0 – 20 min; 100% to 75% A, 20 – 30 min; 75% A to 25% A, 30 – 32 min; 25% A to 100% A, 32 – 35 min.   λ= 240 nm.
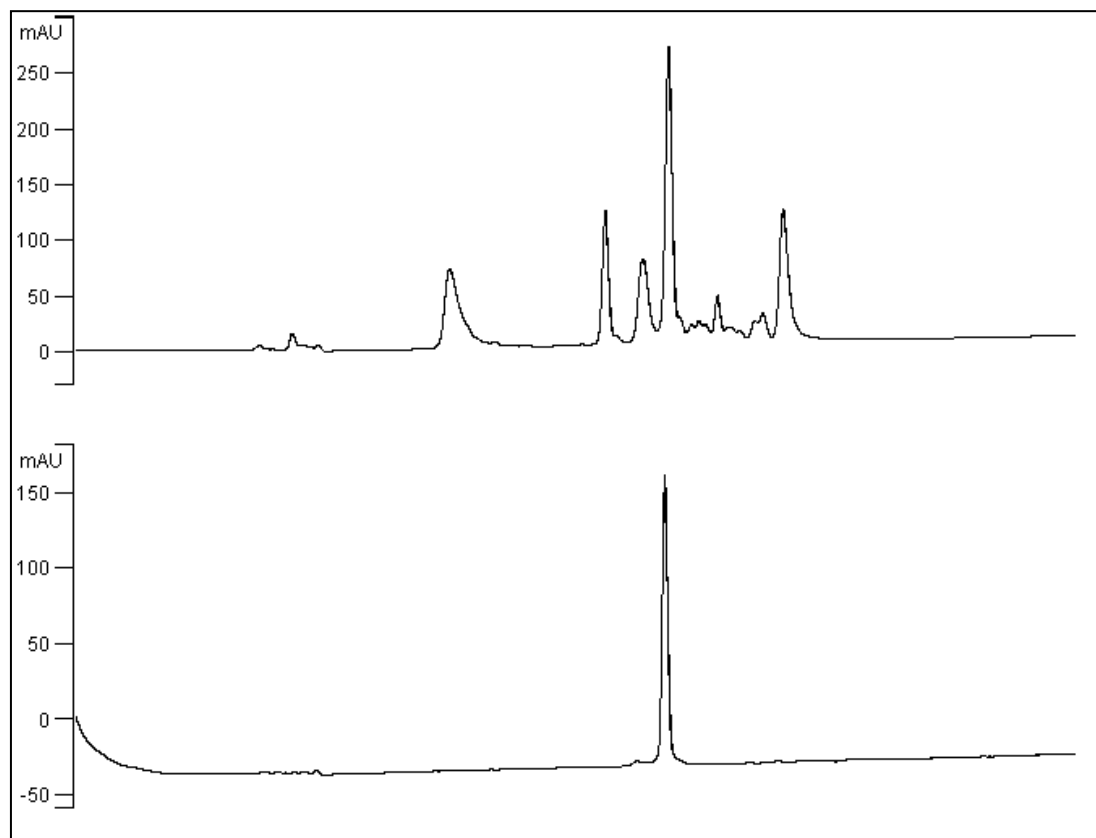
Figure 11 Analytical HPLC chromatogram of crude reaction mixture (top) between insulin and (**2**).The bottom chromatogram shows the HPLC of purified (**4**). Elution Method: A = (CH$_3$CN + 0.1 % TFA), B = (H$_2$O + 0.1 % TFA): Elution Conditions: 25% A to 100% A, 0 – 20 min; 100% to 75% A, 20 – 30 min; 75% A to 25% A, 30 – 32 min; 25% A to 100% A, 32 – 35 min. λ= 240 nm.
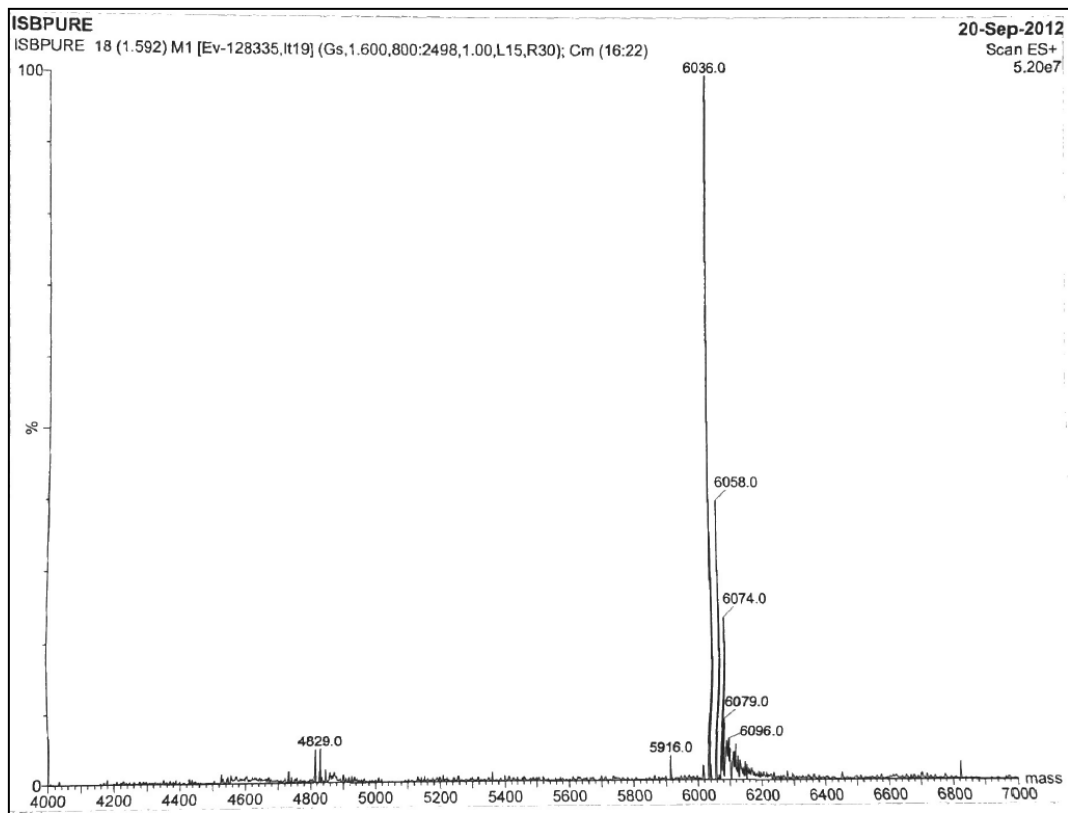
Figure 12 ESI-MS of the peak at t_R= 10.90 minutes which has a m/z value 6036 consistent with the molecular weight of (**3**).
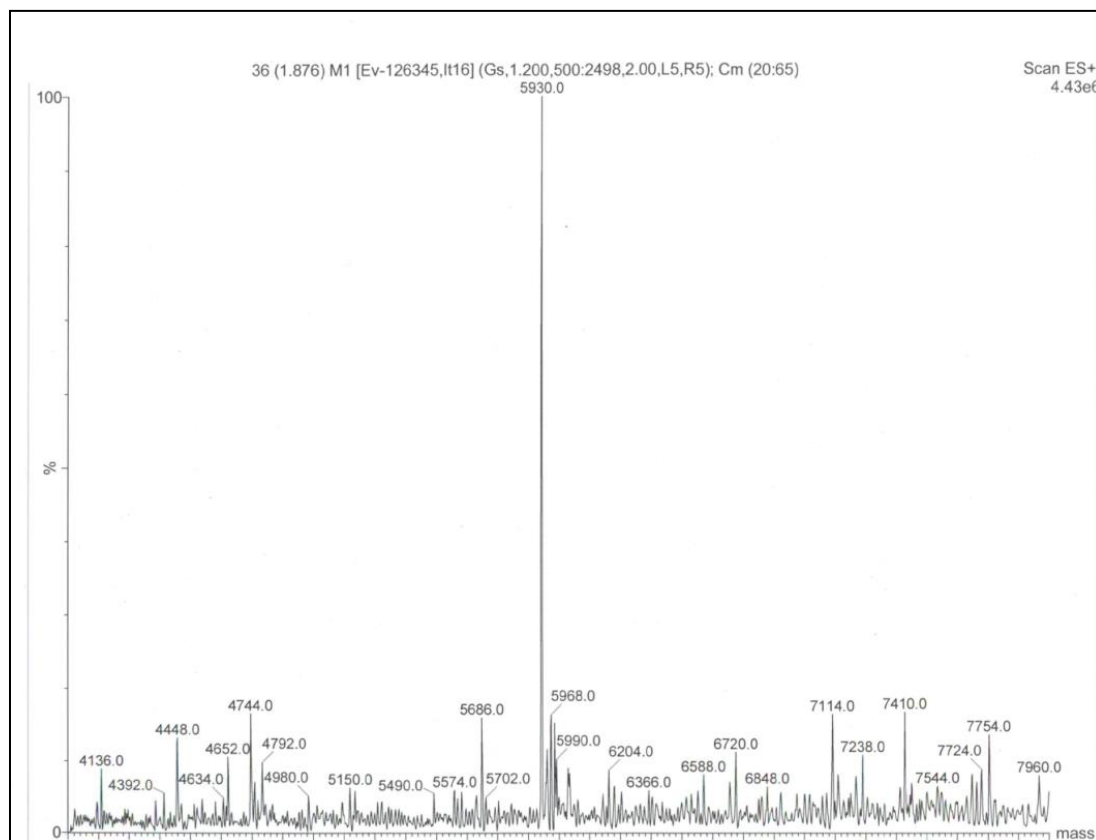
Figure 13 ESI-MS of the peak at t_R= 10.16 minutes which has a m/z value 5930 consistent with the molecular weight of (**4**).

2.3. Confirming the coupling at the B29-Lys position

To determine the site of conjugation, an initial study was performed whereby the retention time of the isolated product (**4**) was compared to an authentic standard of N-[4-fluorobenzoyl]-B1-Phe insulin. This was done since the likely impurity would be the B1-Phe derivative which would not be distinguishable by simple ESI-MS. The products were found to have different retention times (t_R= 10.52 min for the standard, t_R=10.16 min for product (**4**)). These results indicate the derivatization did not occur at the B1-Phe of insulin (Figure 14).
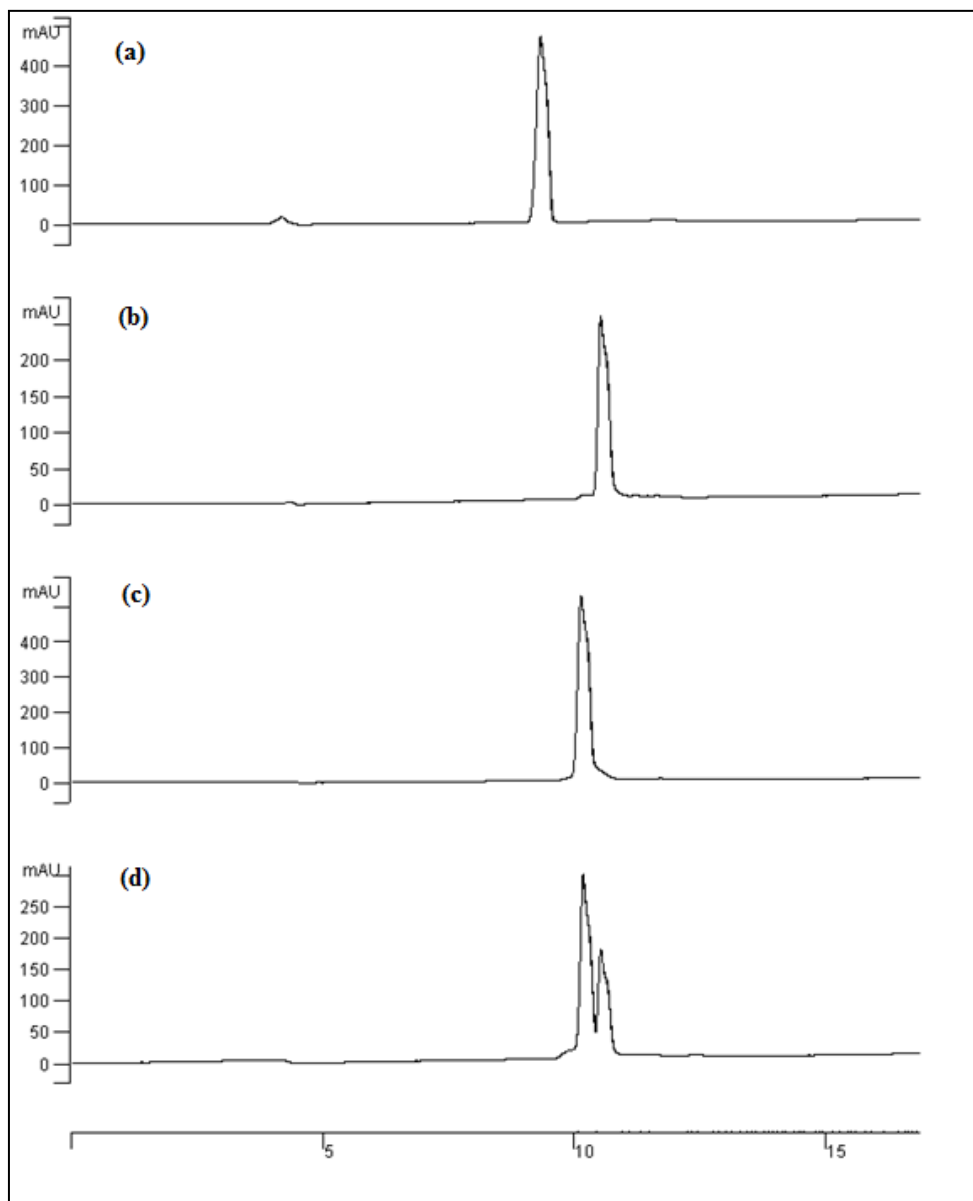
Figure 14 Analytical UV-HPLC (240 nm) chromatograms for (a) Native insulin, (b) N-[4-fluorobenzoyl]-B1-Phe insulin, (c) compound (**4**) and (d) a co-injection of N-[4-fluorobenzoyl]-B1-Phe insulin and (**4**).

2.4. Digestion Experiments

In order to confirm the site of derivatization, a digestion/mass spectrometry protocol was employed. The procedure has been utilized previously to confirm the site of derivatization for insulin derivatives and peptides in general.[35,42,56] Dithiothreitol (DTT)

was used to reduce the disulfide bonds between the two insulin chains separating them into two individual chains that can then be detected by HPLC-MS (positive ion electrospray, ES+) (Figure 15). The second part of the experiment involved sample treatment with endoproteinase-Glu-C (*Staphylococcus aureus* protease V8); a serine proteinase that cleaves amino acid segments at the carbonyl side of glutamic acid. This procedure was used following the DTT treatment and LCMS run to look specifically at B chain fragments (Figure 16).

More specifically, the experimental procedure was initiated with a basic solution of (**4**) that was subsequently treated with aqueous DTT and the mixture incubated for 15 min at 50 °C followed by LCMS (ES+) analysis. The remaining solution from the DTT experiment was then treated with endoproteinase-Glu-C and incubated overnight followed by analysis by LCMS (ES+). Fragments indicative of modified B-chain or unmodified A-chain were not observed for the DTT part of the experiment. The LC-MS (ES+) analysis for the second part revealed a peak with a m/z value of 1239 (Figure 17) which corresponds to the fragment with the amino acid sequence RGFFYTPKT of the B chain plus the pendant fluorobenozate group. There was no evidence of modification of the A-chain (m/z = 2379.7) but there was a small peak corresponding to the unmodified GIVE fragment of the A chain (m/z = 417.2). Based on the LC-MS data and the comparison to the B1-Phe derivatized insulin, the results indicate successful derivatization at the B29-Lys of insulin.
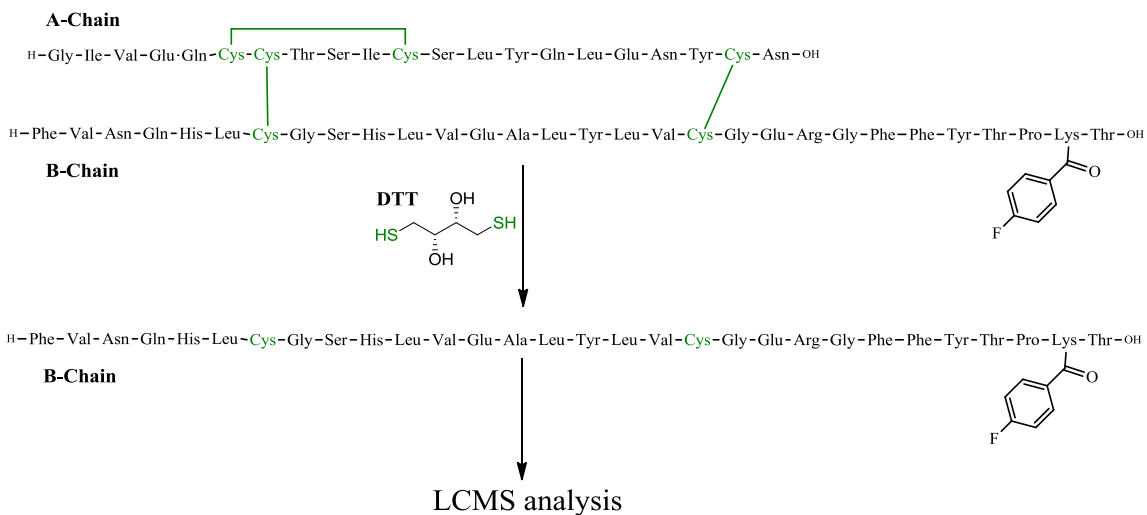
Figure 15 Diagram indicating the use of DTT in the digestion of derivatized insulin (disulfide bonds are highlighted in green).
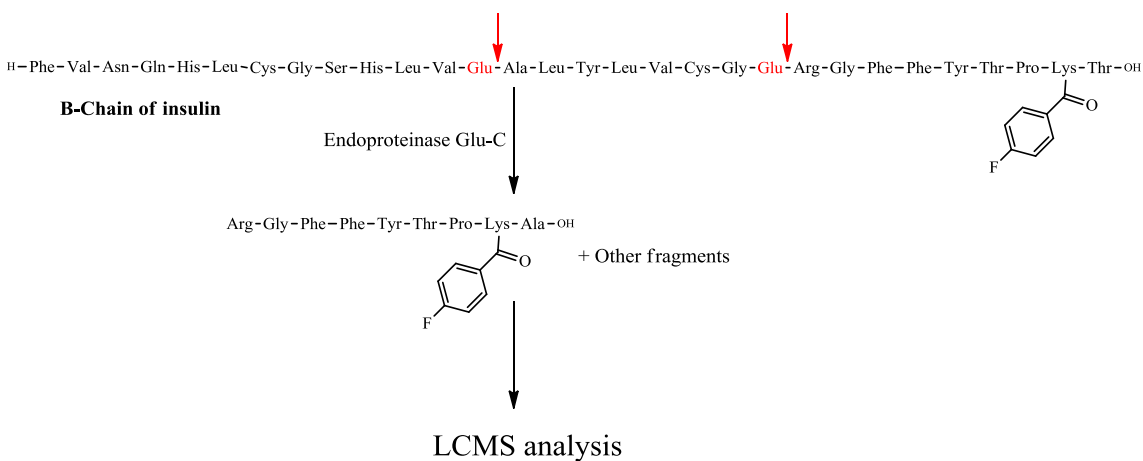
Figure 16 Diagram indicating the use of endoproteinase-glu-c in the digestion of derivatized insulin (red arrows indicate sites of cleavage).
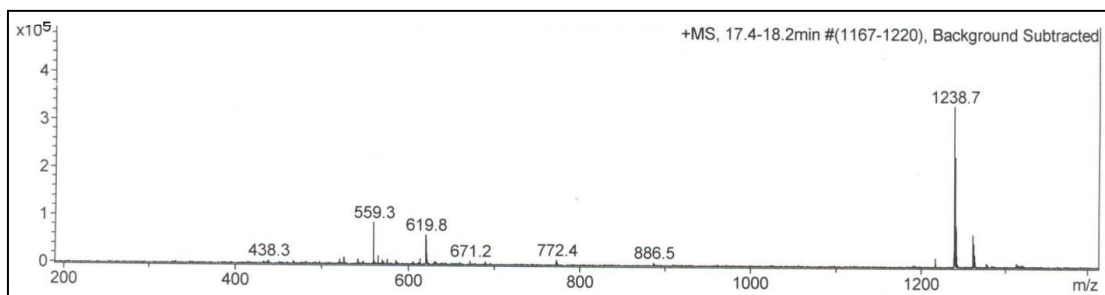
Figure 17 ES-MS chromatogram of a peak at t_R=18.2 min showing a peak (m/z =1238.7) that corresponds to the fragment from the B-chain of insulin (RGFFYTPKT) bearing a fluorobenzoate pendant group.

2.5. IR *in vitro* Competitive Binding Assay

MCF7 human breast cancer cells were used to evaluate IR binding of derivatives

(**3**) and (**4**) using native insulin as a positive control. If successful the resulting IC_{50}

values should be lower than, or at least similar to, that of the unmodified protein. MCF7

cell lines are known for their high IR content which is around 5-fold higher than normal

non malignant cells.[57] To determine the IC_{50} a radioactive assay was performed in which

the concentration of (**3**), (**4**) and native insulin needed for a 50% displacement of [125]I-

insulin (Perkin-Elmer®) were calculated using nonlinear regression analysis. The assay

involves starving MCF7 cells by incubating them overnight prior to starting the assay

with media containing charcoal stripped fetal bovine serum (csFBS). This was done to

deplete the amount of insulin in the cells before exposure to the radioactive insulin probe.

Cells were then incubated with 1 nM ^{125}I insulin in the presence of the competing ligands

((**3**), (**4**) and native insulin) at different concentrations at 4°C for 4 hours in a humid

chamber. This was followed by cell lysis with 1 N NaOH and transfer of the solutions to

gamma tubes for counting.

29

The assay was repeated six times, each in triplicate, where the results indicated that compound (**4**) (IC_{50}=3.6 nM; 95% confidence intervals (CI): 1.869 to 7.135 nM)) has higher affinity for the IR compared to (**3**) (IC_{50}=24.9 nM; 95% CI: 13.7 to 44.7 nM) as indicated by comparison to the IC_{50} values of native insulin tested under the same settings (IC_{50}=1.4 nM; 95% CI: 0.50 to 4.0 nM) (Figure 18). These results show that (**4**) has affinity similar to that of native insulin which was a prerequisite for moving to the next step.
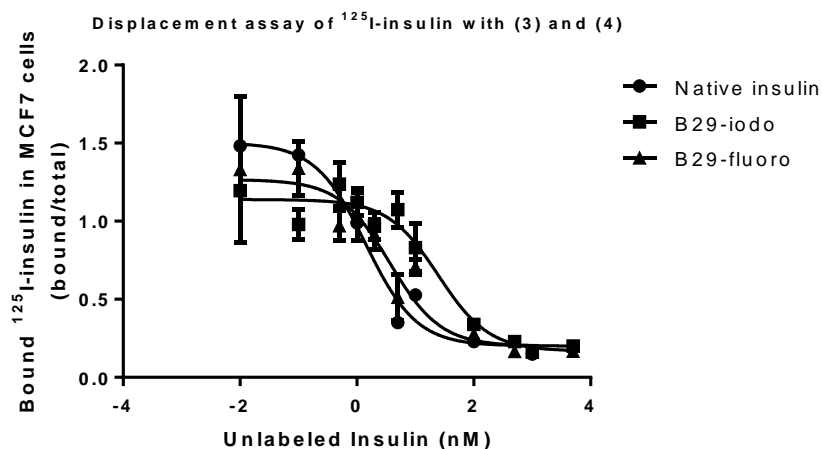
Figure 18 Representative data for displacement assay of ^{125}I-insulin with native insulin (circles), **3** (squares), and **4** (triangles).

2.6. Conclusion

Two new insulin derivatives were prepared using halogenated active esters and the site of derivatization was confirmed using LCMS and a digestion assay. Having established through an *in vitro* assay that (**4**) has high affinity for IR (IC_{50}=3.6 nM; 95% (CI): 1.869 to 7.135 nM) that is comparable to that of native insulin (IC_{50}=1.4 nM; 95%

CI: 0.50 to 4.0 nM) the next step was to prepare the ^{18}F analogue of (**4**). Progress towards producing the radiolabeled insulin derivatives is described in chapter three.

CHAPTER THREE: SYNTHESIS, CHARACTERIZATION and PRELIMINARY STABILITY ASSESSMENT OF ^{18}F LABELED INSULIN

3.1. Synthesis of [18]F N-Succinimidyl 4-fluorobenzoate (6)

The first step in the synthesis of[18]F-labelled N-succinimidyl4-fluorobenzoate (**6**) that can be used to radiolabel insulin was to prepare the quaternary ammonium salt (**5**) (Scheme 3).[55] This salt was ultimately used in a nucleophilic aromatic substitution reaction (S_NAR) to make the active ester. In brief, ethyl-4-(dimethylamino)benzoate was combined with methyl triflate (MeOTf) in dichloromethane (DCM) overnight followed by precipitation from cold ether (Scheme 3). The product was collected by filtration as a white powder in 88% yield. ^{1}H NMR showed two peaks at 8.24 and 7.86ppmwhich are a result of the para substituted nature of the phenyl ring, one quartet at 4.32 ppm corresponding to the methylene protons, a singlet at 3.70 ppm representing the 9 equivalent methyl protons attached to the nitrogen and a triplet at 1.33 ppm for the remaining methyl protons (Figure 19).
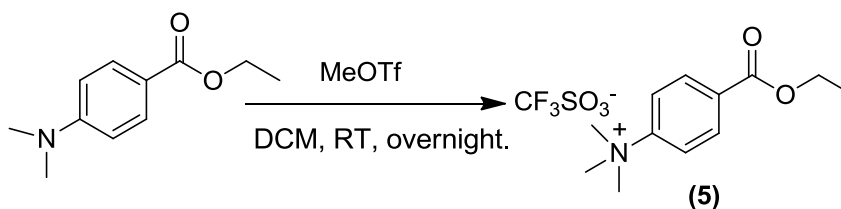
Scheme 3 Synthesis of Ethyl 4-Trimethylammonium Benzoate Trifluoromethanesulfonate (**5**).
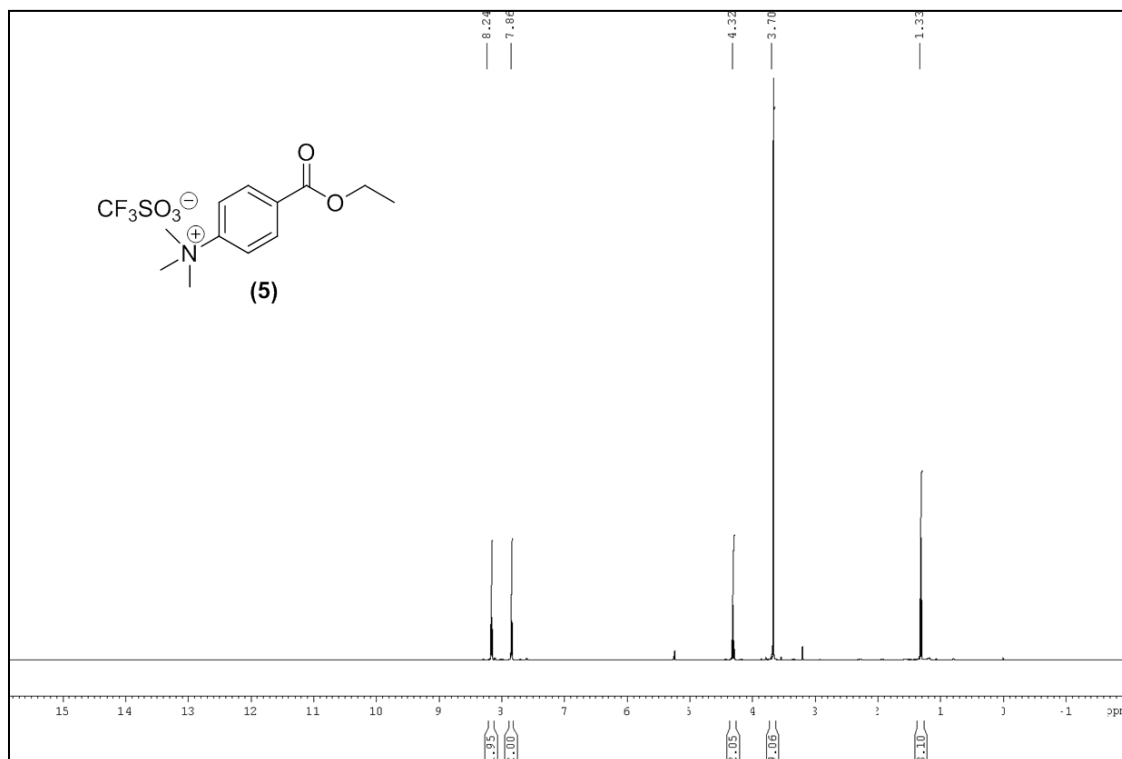
Figure 19 ^{1}H NMR (CD$_2$Cl$_2$, 600.13 MHz) of (**5**).

Scheme [4]) was prepared according to literature procedures.[55] An aqueous K[^{18}F]F

solution was dried *azeotropically* using CH$_3$CN heated to 90 ^{o}C under N$_2$. K[^{18}F]F was

dissolved in DMSO and compound (**5**) was added to the reaction vial at 90 ^{o}C and stirred

for 10 min to produce ethyl-4-[^{18}F]fluorobenzoate. 0.5 N NaOH was added into the

reaction vial at 90 ^{o}C to hydrolyze the ester. After cooling, the reaction mixture was

neutralized with 1 N HCl and water. Tetrabutylammonium hydroxide (TBAOH) was

added to the crude reaction mixture and the desired product eluted from a C-18 Sep-Pak

cartridge and dried under a stream of N$_2$ at 90 ^{o}C as the acid salt. For the last step, the

residue was redissolved in CH$_3$CN and O-(N-succinimidyl)-*N,N,N',N'*-

tetramethyluroniumtetrafluoroborate (TSTU) was added to the reaction vial and the mixture heated to 90 °C for 5 min (

Scheme 4). The desired product (**6**) was purified by HPLC using a semi-preparative column. The desired fraction (t_R= 13.40 min) was collected and dried where the decay-corrected radiochemical yield of (**6**) was between 20-70% (n=7) and the total synthesis time was 120 min including HPLC purification. Identity of the compound was confirmed by co-injecting it with the non-radioactive analogue (**2**) (Figure 20).
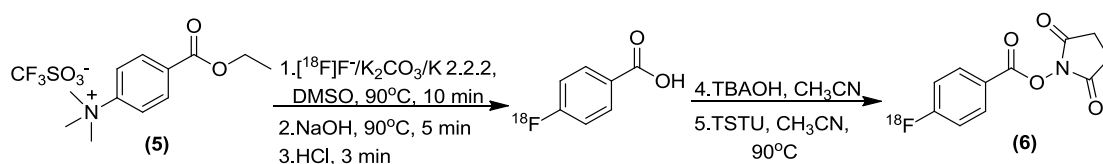
Scheme 4 Preparation of ^{18}F N-succinimidyl 4-fluorobenzoate (**6**).
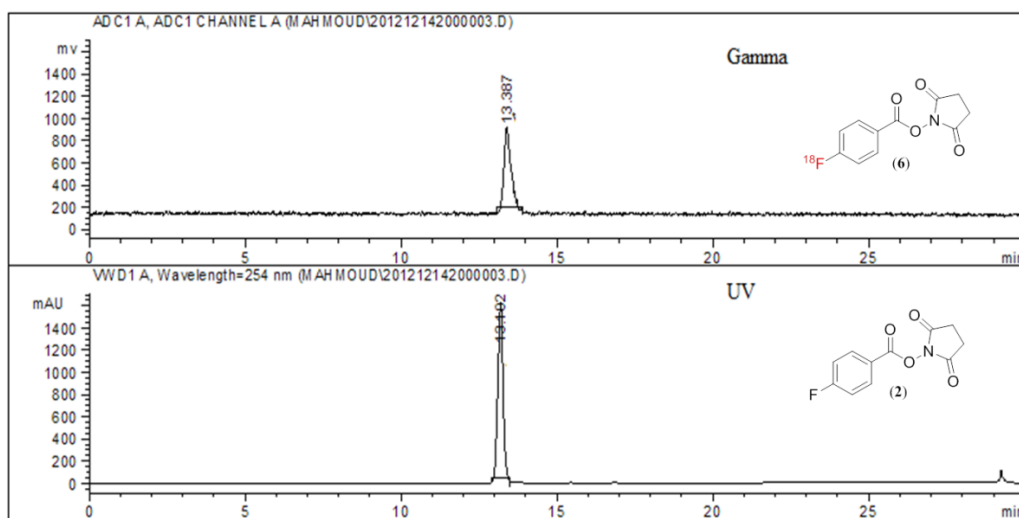
Figure 20 Co-injection of compound (**2**) and purified radiolabeled compound (**6**) which had similar retention times. (λ= 254 nm)

3.2. Radiolabeling insulin with ^{18}F N-succinimidyl 4-fluorobenzoate (6)

The initial approach to labeling was carried out by dissolving insulin and (6) in borax buffer and stirring the mixture at room temperature for 20 min. Unfortunately, no radiolabeled insulin was found in the HPLC traces of the crude mixture and this turned out to be a result of the hydrolysis of the active ester in the borax buffer system. This finding was confirmed by dissolving the dried active ester in the buffer system and re-injecting into an analytical HPLC column where a peak associated with the hydrolyzed benzoic acid was observed. Note that the comparable reaction was not observed when using the cold analogue (4).

Conventional radiolabeling of biological vectors is challenging due to the high cost of the molecules in addition to their sensitive nature which often result in low radiochemical yields, thus new methods are continuously being developed to create suitable reaction environments and increase yields. Emulsion systems are known to accelerate organic reactions possibly via surface effects, preferable orientation of substrates and concentration of reactants (Figure 21). This concept has been utilized recently in radiolabeling of insulin at the B1-Phe position where the results were superior to conventional homogenous solution-based approaches.[45] In the work done to date, DBI was radiolabeled in an emulsion at ambient temperature in yields between 40-80% with no impurities observed. These results support the use of the emulsion based radiolabeling method in preparing the radioactive derivatives of the B29-Lys insulin. To confirm the reliability of the reaction and to refine the experimental technique, labeling of DBI at the B1-Phe position was repeated. The desired product was obtained and purified by semi-

preparative HPLC, dried then formulated in saline (Figure 22). The results were consistent with what was previously reported.
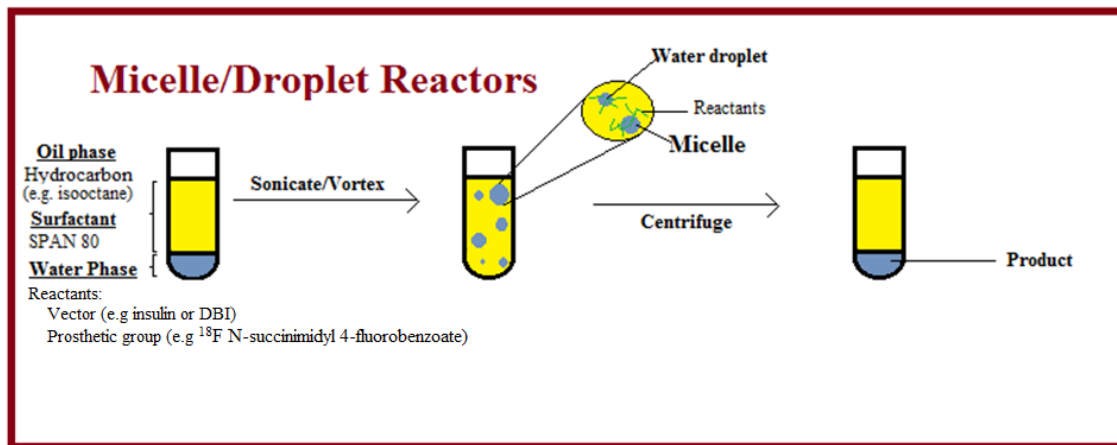
Figure 21 Illustration of the droplet labeling method.
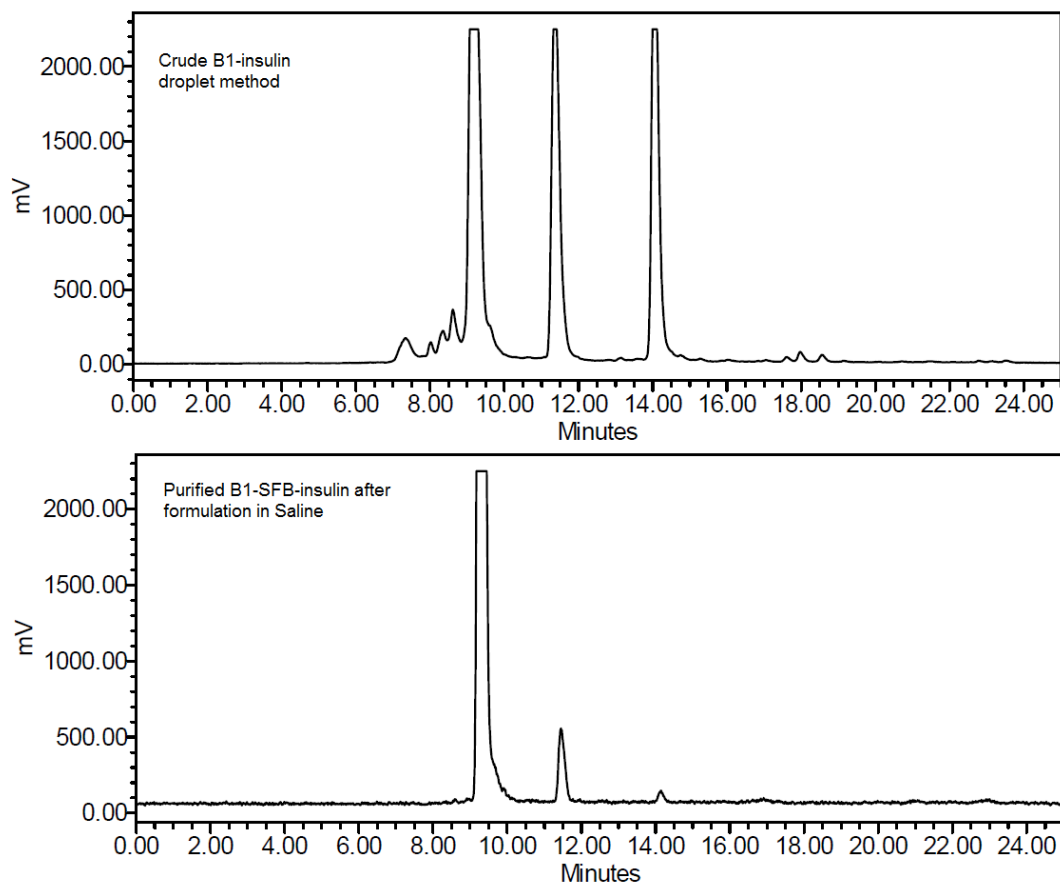
Figure 22 Gamma HPLC chromatograms of B1-Phe-radiolabeled insulin prepared using droplet method; crude reaction mixture (top) and purified product after formulation in saline (bottom).

Several attempts were made to label insulin at the B29-Lys position using the droplet method. Unfortunately, most were low yielding and the procedure favored labeling at other positions. This could be due to the orientation of the B29-Lys away from the oil-water interface which would reduce yield. In light of these results, efforts reverted to employing other more conventional labeling methods.

The most successful labeling conditions were carried out in a mixture of (DMF/water/ 0.1 M NaHCO$_3$) in a ratio of 3:1:1 (v/v/v) where 185-370 MBq (5-10 mCi) of dry (**6**) was dissolved in DMF and transferred to a microwave vial containing 1 mg of

unprotected insulin dissolved in the aqueous $NaHCO_3$ (Scheme 5). The reaction was stopped after 20 minutes and radiolabeled insulin (**9**) (t_R= 8 min) was isolated from the crude reaction mixture using semi-preparative HPLC (Figure 23) and its identity was confirmed by having a similar retention time to the UV peak associated with the co-injected (**4**) (Figure 24).
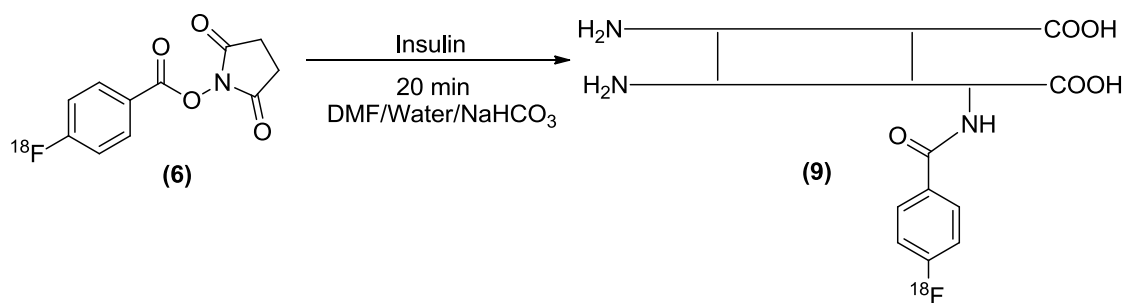
Scheme 5 Synthesis of (**9**) using a conventional labeling strategy.
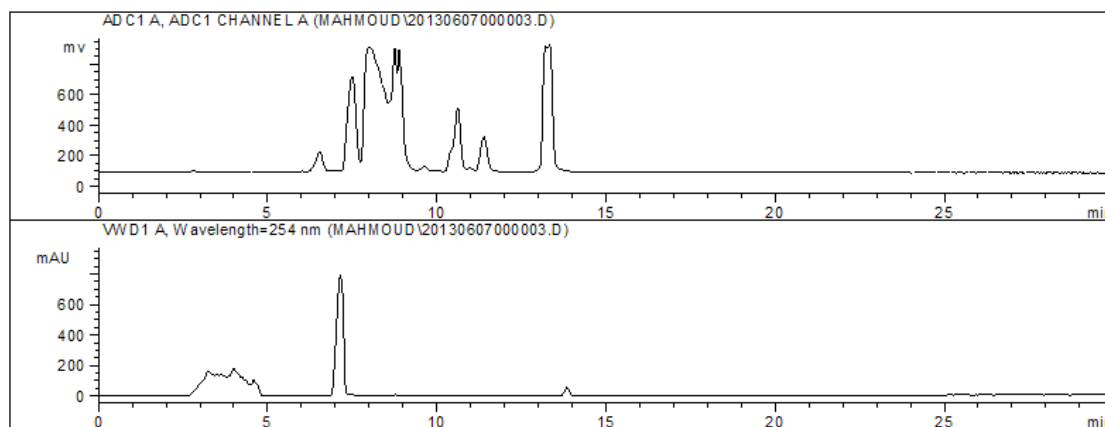
Figure 23 HPLC of the crude reaction mixture for conventional labeling of insulin with (**6**); Gamma trace (top) and UV trace (bottom). (λ= 254 nm)
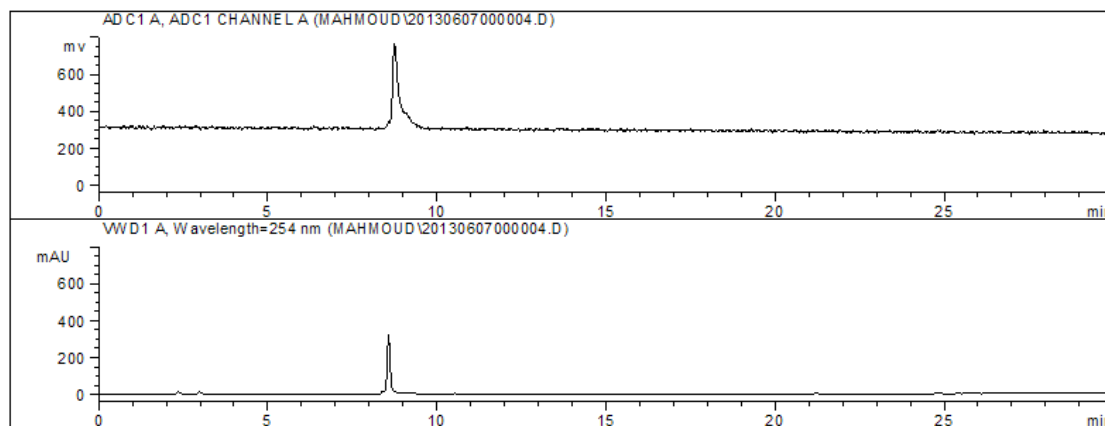
Figure 24 HPLC of the co-injection of purified labeled insulin (**9**) and the non-radioactive insulin analogue (**4**); Gamma trace (top) and UV trace (bottom). (λ= 254 nm).

3.3. Stability studies in saline and PBS

In order to test the stability of (**9**) the agent was dissolved in either saline or PBS, which are used as vehicles for administering radiopharmaceuticals. Radiolabeled insulin (**9**) was dried following HPLC purification where the use of the Biotage evaporation system proved challenging as most of the activity tended to stick to the vials and thus the product could not be reconstituted in the formulating solution. The labeled product was eventually dried using air and two formulations were made; one in saline [7.4 MBq (200 μCi)] and one in PBS [9.25 MBq (250 μCi)]. The labeled insulin was shown to be stable for up to four hours in both saline (Figure 25) and PBS (Figure 26). It is also noteworthy that cold insulin was present in the samples as shown in the UV traces as separation of the two compounds by HPLC proved difficult.
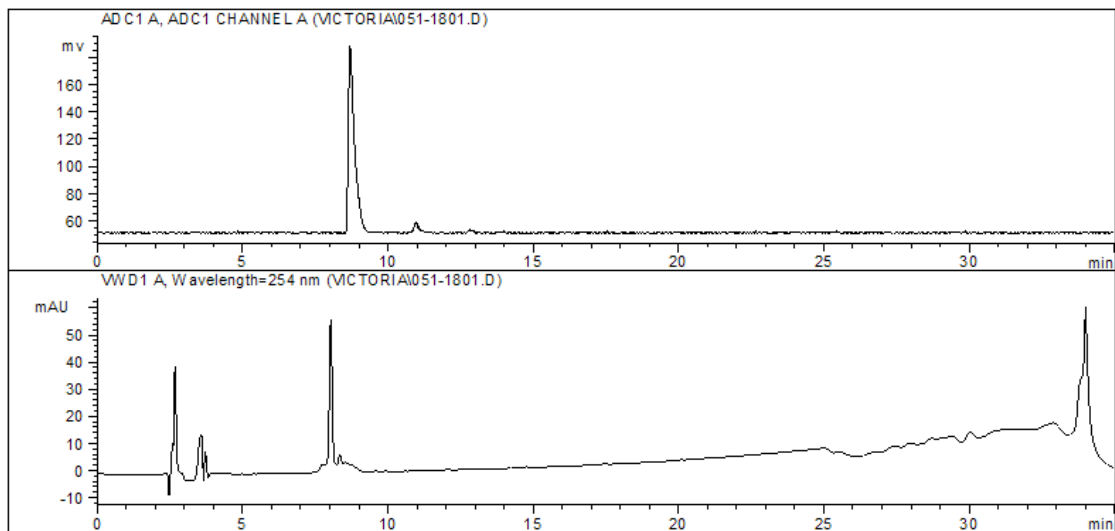
Figure 25 Analytical gamma HPLC chromatogram for radiolabeled insulin (**9**) (top); 4 hours post formulation in saline and UV tracer (bottom) showing unlabelled insulin. (λ= 254 nm)
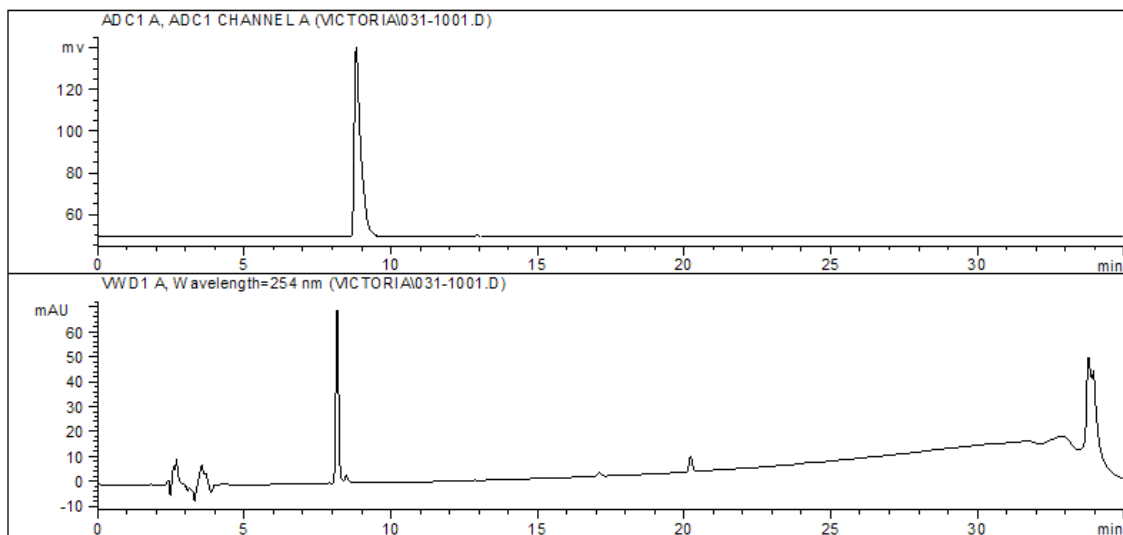
Figure 26 Analytical gamma HPLC chromatogram for radiolabeled insulin (**9**) (top); 3 hours post formulation in PBS and UV tracer (bottom) showing unlabelled insulin. (λ= 254 nm)

3.4. Summary

A radiolabeled form of insulin bearing a prosthetic group at the B29-Lys position

was synthesized. The non-radioactive analogue showed high affinity for the IR. The

product represents a new candidate probe that has the potential to be used to image IR

expression with PET. During the course of this work, experiments performed in our laboratory with ^{18}F-labeled B1 insulin showed that the metabolic stability and circulation time of the agent was as critical as affinity for achieving optimal biodistribution results *in vivo*. As a result the emphasis shifted to evaluate an approach to addressing these issues prior to testing (**9**) *in vivo*.

3.5. Increasing circulation time and reducing metabolism

A key challenge when developing insulin based nuclear imaging probes or insulin based pharmaceuticals in general is the pharmacokinetic profile of the parent ligand. The innate properties of the hormone itself along with its peptidic nature make it susceptible to degradation by both specific mechanisms like the insulin degrading enzyme (IDE) and general peptidases found in the plasma.[58] Several strategies can be implemented towards addressing this issue where the use of long chain fatty acids and 6-fluoronicotinic acid were investigated here.

3.6. Palmitic acid and myristic acid B-29 acylated insulin

Long chain fatty acids can be used as a way of modifying insulin's pharmacokinetic profile by increasing its biological half-life and duration of action. Insulin acylated at the B29-Lys with long chain fatty acids, which promote albumin binding in the blood, resulted in a sustained delivery of insulin.[59] B29-Lys myristic acid acylated insulin for example, which is known as insulin Detemir, is used for the treatment of diabetes (Novo Nordisk). Insulin has also been derivatized with palmitic acid with similar results.[48] Implementing a comparable prosthetic group bearing a radiolabel could prolong the circulation time of an insulin derived probe, overcome the

problems associated with premature degradation and maximize delivery to the target (tumours).

To optimize synthetic strategies and test the impact of the prosthetic groups on IR binding, N-[myristoyl]-(B29-Lys) insulin (**7**) and N-[palmitoyl]-(B29-Lys) insulin (**8**)were synthesized in a similar fashion to (**3**) and (**4**) (Scheme 6). The products, which were purified by semi-preparative HPLC (method A) (Figure 27) in 48%theoretical yield, were subsequently screened for IR binding. The assay results indicated that the average IC_{50} values for these compounds were 196.0 nM (95% CI: 105.6 to 363.5 nM) for (**7**)) and 577.9 nM (95% CI: 309.0 to 1110.0 nM) for (**8**) which is significantly higher when compared to the IC_{50} value of native insulin evaluated in the same experimental setting (9.1 nM; 95% CI: 5.0 to 165 nM). These results suggest a negative effect on IR binding which is a key requirement for a successful MI probe. In light of these results further work on these molecules was not pursued.
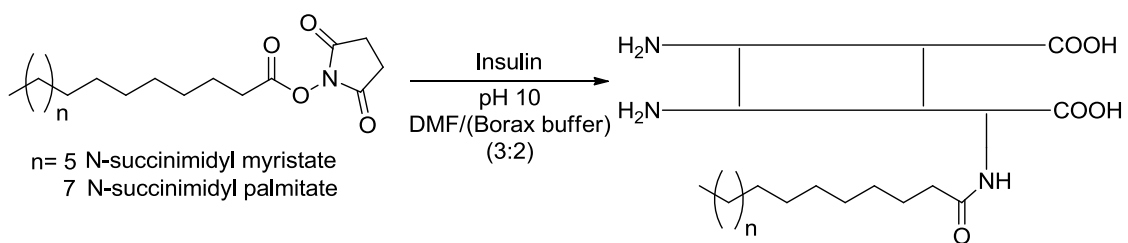
Scheme 6 Synthesis of fatty acid acylated insulin, compounds (**7**) and (**8**).
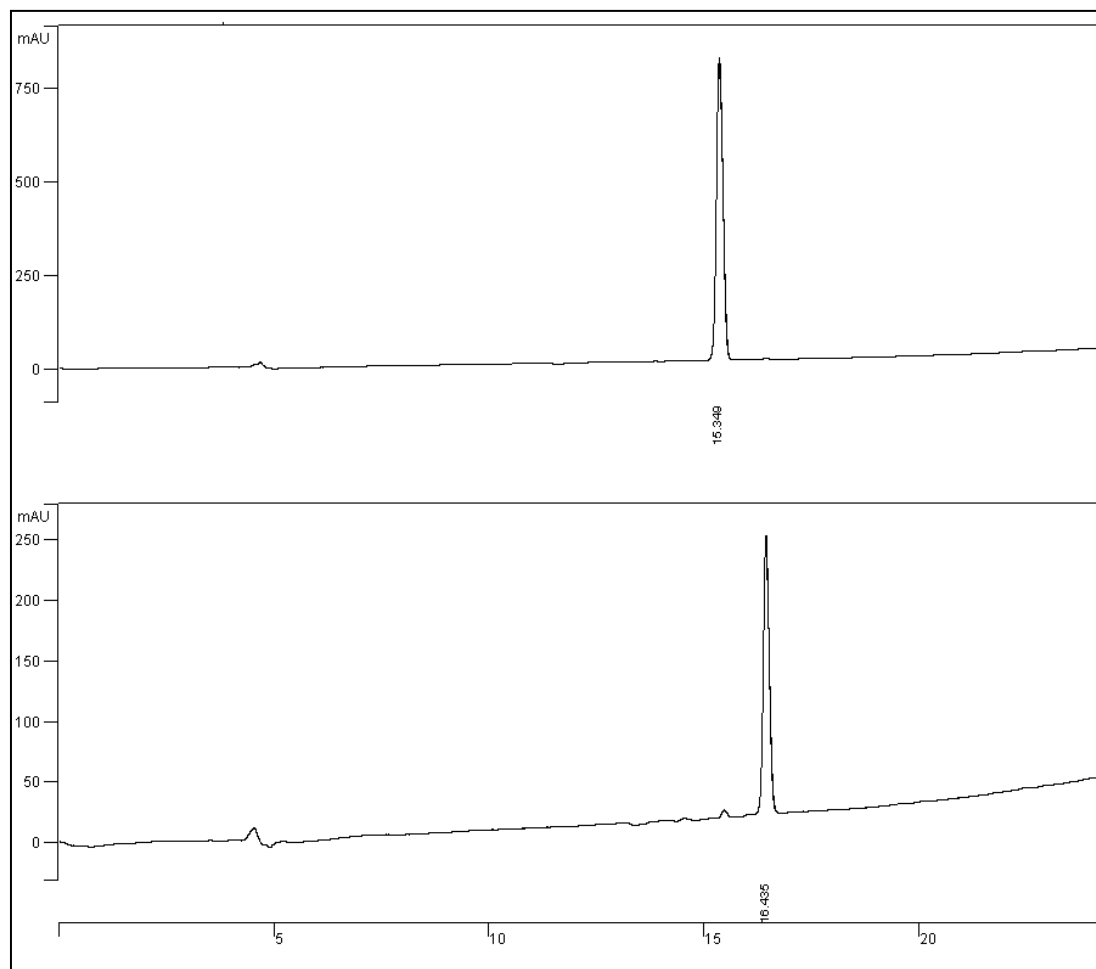
Figure 27 Analytical HPLC spectra of purified (**7**, t_R=15.3) (top) and (**8**, t_R=16.4) (bottom). (λ= 240 nm)

3.7. Acylation with 6-Fluoronicotinic acid

The second strategy implemented to modify insulin's pharmacokinetic profile and to enhance tumour uptake was to tag insulin with 6-fluoronicotinic acid instead of the 6-fluorobenzoic acid used in previous chapters. 6-Fluorobenzoic acid has been used to improve residualization of molecules inside the cells, which is favorable in the design of radiopharmaceuticals as it facilitates tumour saturation.[60] [18]F nicotinic acid derivatives have displayed high tumor uptake including up to 17% ID/g in melanoma tumours.[61] The

42

key here is that the basicity of the pyridine nitrogen promotes entrapment intracellularly due to protonation of the pyridine nitrogen. It is also worth mentioning that Cuthbertson *et al.* efficiently synthesized the ^{18}F tetrafluorophenol (TFP) active ester of 6-fluoronicotinic in a one-step radiosynthesis reaction which is more convenient when compared to the two step radiosynthesis of the NHS ester of 6-fluorobenzoic acid.[62]

Following a modified literature procedure, non-radioactive 6-fluoronicotinicacid 2,3,5,6-tetrafluorophenyl ester (**10**) was chosen for the B29-Lys conjugation.[62] The compound was synthesized in yields between 60-70% and the reaction was carried out by dissolving6-fluoronicotinicacidin DCM followed by addition of TFP and dicyclohexylcarbodiimide (DCC) with stirring overnight (Scheme 7). The desired product was isolated by filtration to remove the urea byproduct followed by re-crystallization from hot hexane. Identity of the molecule was confirmed by mass spectrometry (EI-MS) indicating a m/z ratio of 289.0 (Figure 28) and ^{1}H NMR spectroscopy which showed signals corresponding to the one aromatic proton on the phenyl ring and peaks at 7.16, 8.60, and 9.12 ppm corresponding to the protons on the pyridine ring (Figure 29).
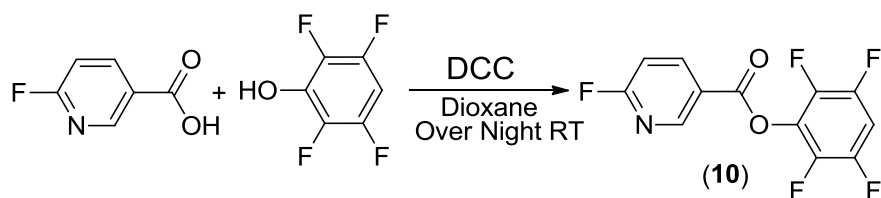
Scheme 7 Synthesis of the non-radioactive 6-fluoronicotinicacid 2,3,5,6-tetrafluorophenyl ester (**10**).
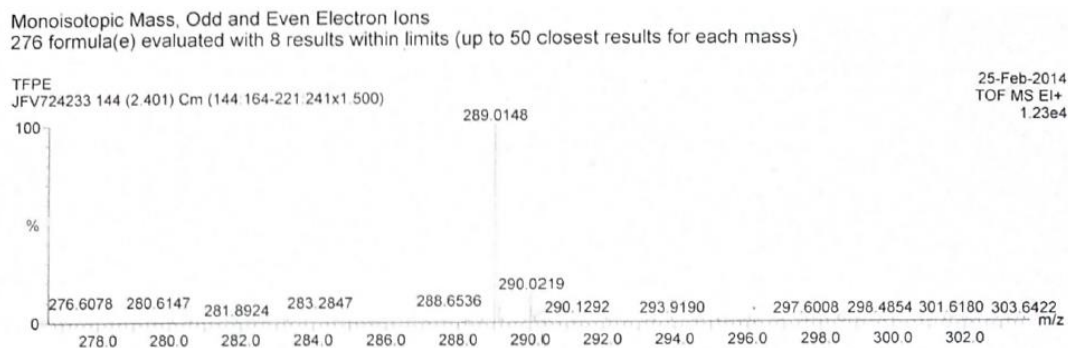
Figure 28 EI-MS spectrum for pure 6-fluoronicotinicacid 2,3,5,6-tetrafluorophenyl ester (**10**).
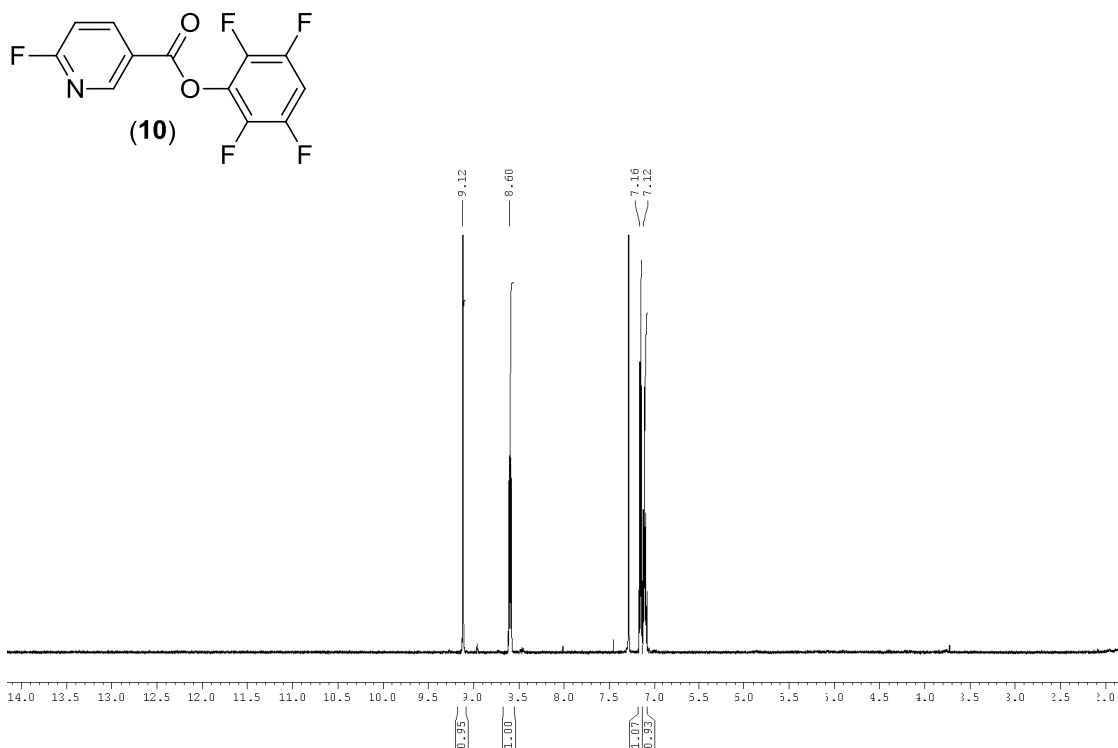
Figure 29 ^{1}H NMR (CDCl$_3$, 600.13 MHz) of 6-fluoronicotinicacid 2,3,5,6-tetrafluorophenyl ester (**10**). Residual CHCl$_3$ can be seen at 7.24 ppm.

N-[6-Fluoronicotinyl]-(B29-Lys) insulin (**11**) was synthesized in a similar fashion to (**3**) and (**4**) by reaction of insulin and (**10**) in a mixture of borax buffer and DMF for 30 minutes at pH 9.96 (Scheme 8). The product was purified by semi-preparative HPLC in

94% purity (Figure 30) and ESI-MS showed a m/z ratio of 5931.0 (Figure 31) for the

purified product.
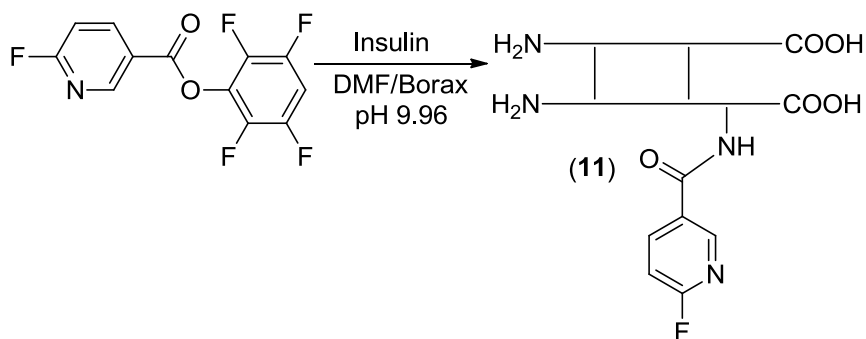
Scheme 8 Synthetic scheme for N-[6-fluoronicotiniyl]-(B29-Lys) insulin **(11).**
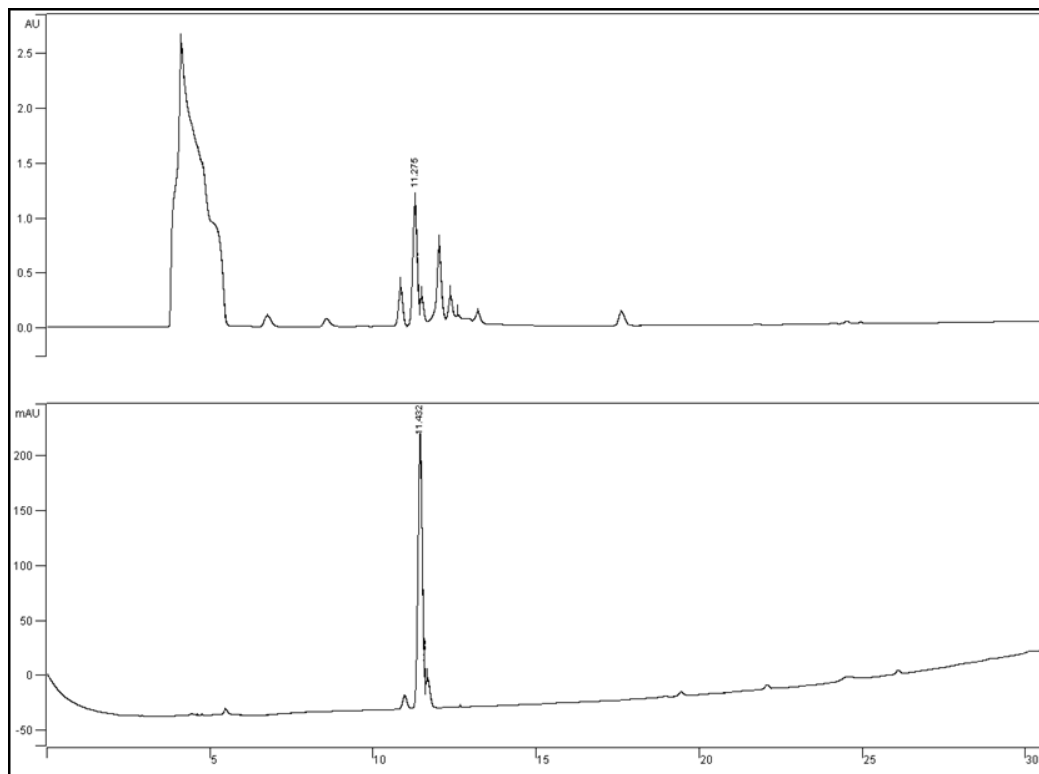
Figure 30 Analytical HPLC chromatogram of crude reaction mixture (top) and purified product **(11)** (bottom). Elution Method: A = (CH$_3$CN + 0.1 % TFA), B = (H$_2$O +0.1 % TFA): Elution Conditions: 25% A to 100% A, 0 – 20 min; 100% to 75% A, 20 – 30 min; 75% A to 25% A, 30 – 32 min; 25% A to 100% A, 32 – 35 min.   (λ= 240 nm)
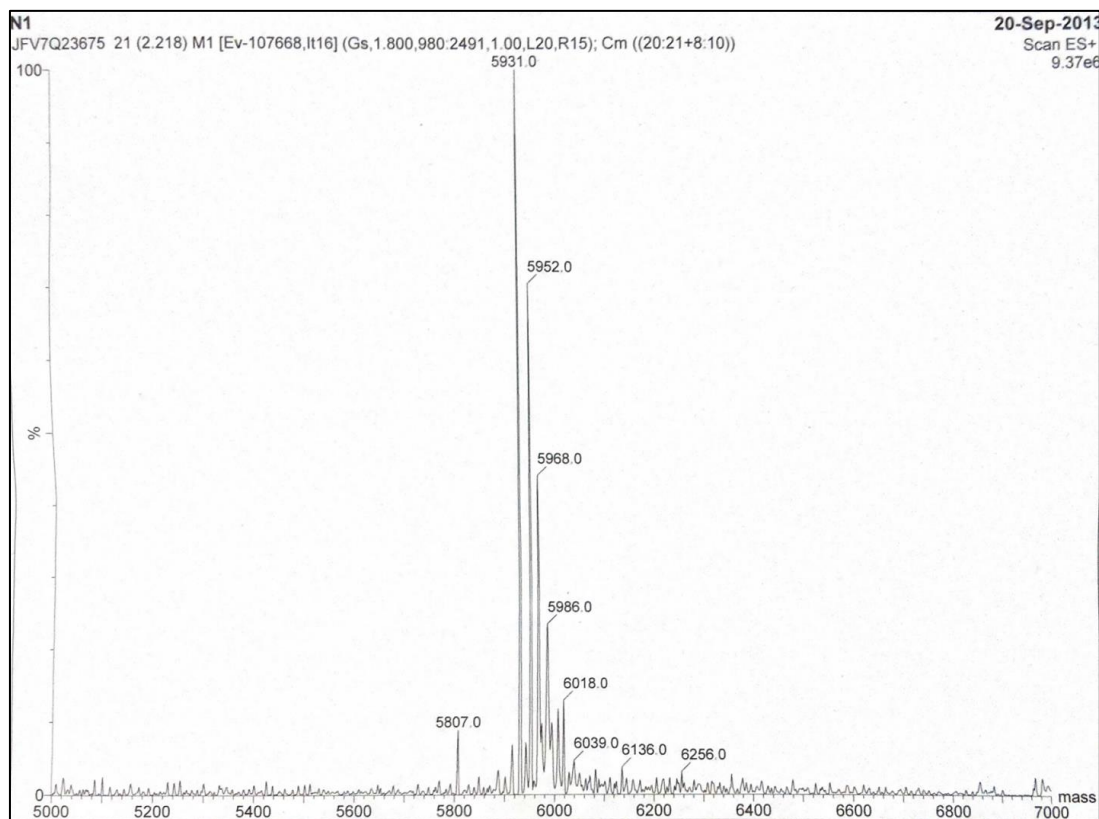
Figure 31 ESI-MS of the peak with t_R= 11.40 minutes which has a mass of 5931.0 m/z consistent with the molecular weight of (**11**).

The digestion/mass spectrometric protocol described in chapter 2 was conducted using (**11**) in order to confirm the identity of the monosubstituted species. Fragments indicative of modified B-chain and un-modified A-chain were not observed for the DTT part of the experiment and this is probably due to using a lower concentration of DTT thus fragments of intact disulfide bridges were expected to be found following endoproteinase-Glu-C treatment. A fragment of the modified B29-Lys position did not show following LCMS (ES+) analysis but two other fragments indicating unmodified A-chain GIVE fragment (at a m/z of 417.2) and unmodified B1-Phe position QCCTSICSLYQLE-FVNQHLCGSHLVE fragment (at a m/z of 1485.63 (M/2)) were

46

found (Figure 32) providing some evidence that the modification occurred at the B29-Lys position.
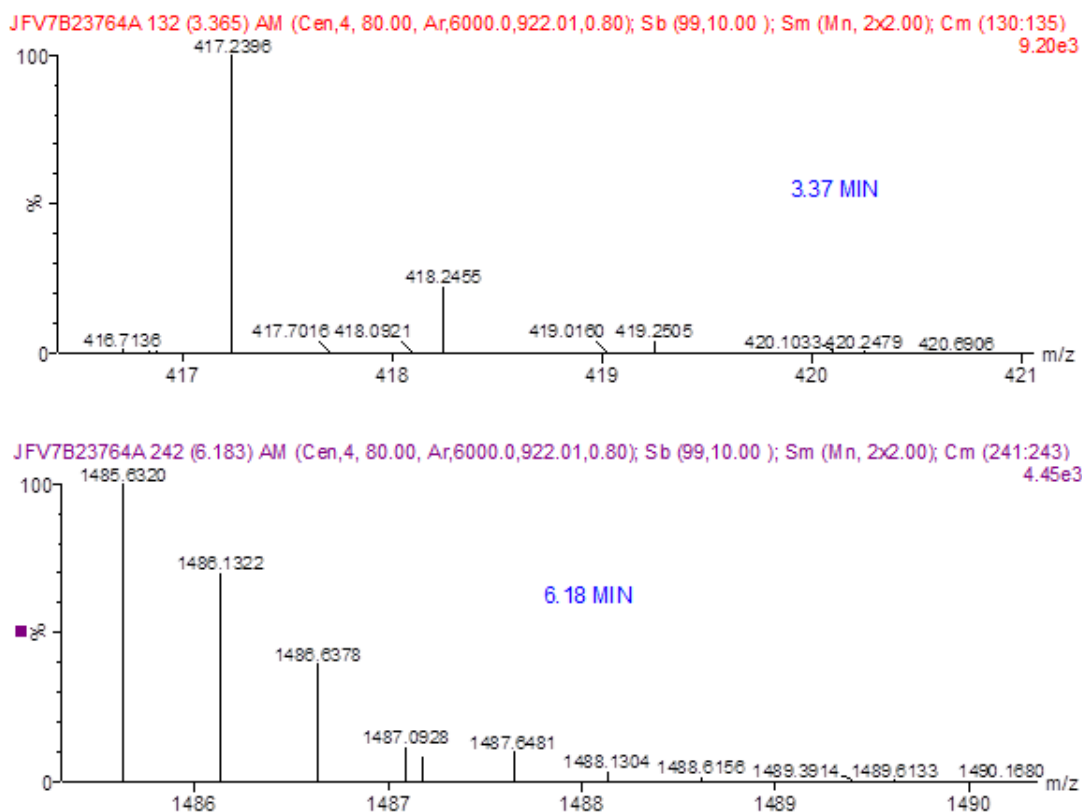
Figure 32 Detected fragments following LCMS (ES+) digestion protocol on (**11**).

N-[6-fluoronicotiniyl]-(B29-Lys) insulin (**11**) was screened for *in vitro* IR binding using the ^{125}I insulin displacement assay. Three consecutive screens using MCF7 cells to assess IR binding of (**11**) derivative were completed with a single lot of ^{125}I insulin. As a reference, the combined aggregate data for human recombinant insulin for these experiments resulted in an IC_{50} of 6.9 nM (95% CI: 5.0 to 9.5 nM). The IC_{50} of (**11**) was 30.1 nM (95% CI: 20.1, 45.0 nM), approximately 4.2 times that obtained for native insulin in the same assay.

Based on the IR binding data for (**11**), it was worth investigating how different the IC_{50} values would be compared to the structurally similar B1-Phe acylated derivative, especially when the B1-Phe fluorobenzoate derivative previously reported by Kim *et al.* showed better IC_{50} values compared to the B29-Lys derivative (**4**) reported in chapter 2. Attempts to derivatize DBI with (**10**) were conducted following literature procedure but the crude reaction mixture showed a single broad peak when analyzed by HPLC and following mass spectrometric analysis a small molecular weight adduct made it difficult to isolate the desired product.[35]

In light of the challenges with the TFP ester, an NHS ester of 6-fluoronicotinicacid was used subsequently. To ensure the DBI reaction was performing as previously reported, a proof of concept experiment was performed using N-[4-fluorobenzoyl]-(B1-Phe) insulin was undertaken. The product was successfully synthesized and purified in accordance with the literature procedure (Scheme 9). The N-succinimidyl ester of 6-fluoronicotinic acid was synthesized in a similar fashion to the fluorobenzoate esters (Scheme 10), but it required extensive re-purification and signals corresponding to starting materials were always present in the ^{1}HNMR spectrum. For these reasons, the decision was made to not make any further progress on this project.
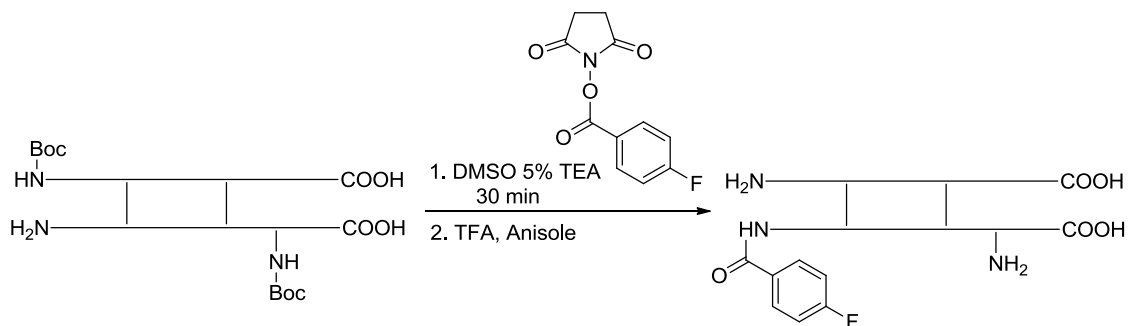
Scheme 9 Synthesis of N-[4-fluorobenzyl]-(B1-Phe) insulin.
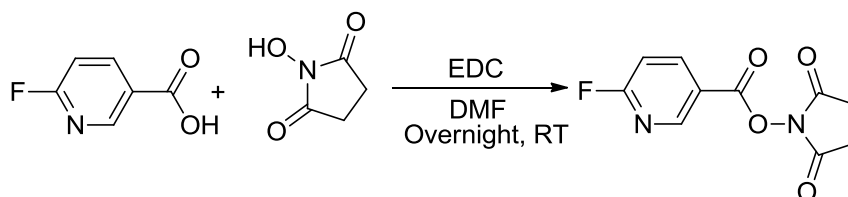
Scheme 10 Synthetic scheme for N-succinimidyl ester of 6-fluoronicotinic acid.

3.8. Conclusions and Future Work

Several approaches were undertaken to prepare B29-Lys labeled insulin. The most promising was conventional labeling at room temperature in water and $NaHCO_3$ with ^{18}F where the desired product was obtained in 20% yield. The cold analogue had an IC_{50} of 3.6 nM (95% CI: 1.869 to 7.135 nM) which was comparable to insulin. Next steps should focus on assessing the plasma stability of (**9**) and performing biodistribution studies in both normal mice and mice bearing IR expressing tumours.[63]

Additional efforts were made to modify insulin to enhance uptake and reduce metabolism; unfortunately the synthetic strategies were either unsuccessful or produced compounds with low IR affinity. These issues likely have to be addressed before a viable probe for imaging IR expression on breast cancer can be developed. As a result of these

challenges work shifted to a promising new probe development technology that arose in our group (US molecular imaging) and a target (uPAR) whose expression is directly linked to tumour aggressiveness. This work is presented in chapter four.

CHAPTER FOUR: PREPARATION AND SCREENINGOF uPAR TARGETING MICROBUBBLES USINGBIOORTHOGONALCHEMISTRY

4.1.Overview

The ultimate goal in designing any cancer imaging probe is to be able to effectively detect tumour cells and differentiate them from healthy ones. There is a further need to be able to stratify tumours based on their metastatic potential. The value of such a probe is particularly significant when it comes to detection of breast cancer. In the previous chapters efforts were made to use insulin as a platform for such an agent based on the fact that the IR is overexpressed in breast cancer tissue. Given the challenges in radiolabeling and poor tumour uptake *in vivo*, the focus shifted to imaging a new target using US in place of nuclear imaging methods.

4.2.uPAR in Cancer

uPAR is a heterogeneously glycosylated, single-chain polypeptide of molecular weight of 50-60 kDa, which decreases to 35 kDa upon deglycosylation.[64] It is a member of the lymphocyte antigen (Ly-6)/uPAR protein family that is involved in regulation of tissue plasminogen with a variety of ligands, such as urokinase-type plasminogen activator (uPA), which plays a key role in cell adhesion, migration and proliferation.[65,66]

Under normal physiological conditions, the cellular expression of uPAR is low and it increases under specific conditions including tissue remodeling, inflammation, and immune response.[67] It has also been found that uPAR expression is high in select pathological conditions like chronic kidney disease, ischemic injury, the central nervous

system (CNS) and most importantly cancer.[68–70] uPAR expression is elevated in different forms of cancer including solid tumors, bone marrow and blood stem tumours, lymphomas and stromal cells such as fibroblasts and tumour associated macrophages.[70–73] High tumour tissue mRNA expression is associated with clinical outcomes indicating faster metastasis and decreased overall survival in breast cancer patients.[74] Fibroblastic expression of uPAR was also found to be an independent prognostic factor of patients' shortened relapse-free survival.[75] The role of the uPA/uPAR system in facilitating cancer metastasis – although not yet fully understood – can be attributed to its involvement in the degradation of extra cellular matrix (ECM). Binding of pro-uPA, the inactive form of uPA, to uPAR boosts the conversion of pro-uPA to active uPA which consequently converts plasminogen to active plasmin. It is this active plasmin that degrades ECM/basement membrane and releases active meta-metalloproteinases (MMPs), which play a key role in cancer cell invasion and metastasis.[66,76]

uPAR is a promising target for *in vivo* visualization with molecular imaging as it would allow for determination of the metastatic potential of the tumour being examined, which will consequently affect treatment choices for the patient. One other advantage of having a uPAR-targeted molecular imaging probe is that it will overcome the current limitations associated with obtaining tissue samples through biopsy, which is the current method employed for quantifying uPAR expression.

Several uPAR targeted probes can be found in the literature; optical, MRI, nuclear and multimodality imaging probes were all designed to evaluate the expression

of uPAR *in vivo*. One example of an optical probe targeting uPAR implemented a semi-automated approach to correlate two-dimensional (2D) noninvasive near-infrared fluorescence (NIRF) imaging with three-dimensional (3D), high-resolution, flat-panel volume computed tomography (fpVCT).[77] Anti-uPAR antibodies labeled with a fluorescent cyanine dye (Cy5.5) were used to visualize human mammary cancer MDA-MB-231 xenograft in mice and a strong correlation between tumour size and florescence intensity was observed.

Utilizing the advantageous anatomical resolution of MRI, a recombinant peptide derived from mice targeting uPAR was conjugated to magnetic iron oxide nanoparticles where high and specific uptake was observed in uPAR-expressing cells.[78] Unfortunately, interspecies variations between humans and mice could limit the utility of this construct.

Nuclear imaging probes targeting uPAR for both SPECT and PET imaging have also been reported. One example is an anti-uPAR[111]In-labeled peptide designed as a potential probe for SPECT imaging.[79] The probe showed uPAR binding IC_{50} values 300 fold higher than that of uPA itself, which played a key factor in the biodistribution results as endogenous uPA competed with the labeled peptide. This conclusion was drawn by comparing *ex vivo* and *in vivo* data. Several attempts to develop a PET probe targeting uPAR have also been reported. For instance, a ^{64}Cu-labeled high-affinity anti-uPAR peptide was evaluated in a mouse tumour model bearing uPAR-positive U87MG human glioblastoma where the tumour uptake was 10-fold higher than that in the negative cell line (MDA-MB-435 cells).[80] In fact, this interesting high-affinity uPAR peptide

53

antagonist probe (known as ^{64}Cu-DOTA-AE105) was evaluated in a quantitative PET study,[81] and it is currently being evaluated in human clinical trials.[82] LeBeau *et al.* recently reported the use of two humanized anti-uPAR antagonistic antibodies for both *in vitro* and *in vivo* studies.[83] *In vitro* results indicated that both of these antibodies can bind efficiently to the surface of MDA-MB-231 uPAR expressing cells, as evident from a uPAR staining fluorescent study. *In vivo,* SPECT images and near-infrared optical images of the ^{111}In labeled antibodies confirmed the ability to detect uPAR expression in triple negative breast cancer tumour xenografts.

4.3. US Imaging

US imaging, or ultrasonography, is an imaging modality that is performed by signal processing of the reflections of sound waves directed towards the tissues within the body.[84] It is the most routinely used imaging modality in current medical practice due to the fact that it is noninvasive, safe and is available at a low cost.[85,86] US is not restricted to diagnostic applications, as it is also used for biopsy guidance and tissue ablation through the use of high-intensity focused US (HIFU).[86,87]

4.4. Contrast Enhanced US Imaging Using Targeted Microbubbles (MB)

Small gas filled bubbles, otherwise known as MBs are used to enhance US imaging. MBs typically have a diameter of 1–10 μm, and are designed to oscillate when exposed to ultrasonic pulses that can be deflected to a vessel wall, thus enhancing the reflectivity of perfused tissues.[88] Several non-targeted MBs such as Definity® (Lantheus

Medical Imaging, Inc.) are already approved for use in humans for imaging of the myocardium.[89] They are also being intensively investigated as a tool for drug delivery.[86]

Targeted US imaging use MBs bound to a ligand that has high affinity for a specific receptor expressed at the site of disease.[85] Typically, targeted MBs are prepared by attaching an antibody or analogous vector by surface conjugation to the MB through streptavidin-biotin interactions or covalent bonds. Key examples include antibody and peptide functionalized MBs targeting angiogenesis and integrins that are designed to bind vascular endothelial growth factor receptor 2 (VEGFR2) $\alpha_v\beta_3$ integrin respectively. [90,91] One of the challenges with this approach is the difficulty in reproducibly producing modified MBs and in finding ligands that can effectively target the cell-sized constructs.

4.5. Targeted Bubbles using Bioorthogonal Chemistry

Bioorthogonal chemistry involves chemical reactions that are highly selective, biocompatible and are capable of linking two xenobiotics in a living system.[92] This chemistry has important applications in chemical biology, molecular imaging and medicine.[93] Copper-free click chemistry reactions are often employed in bioorthogonal chemistry where one prominent example is the inverse-electron-demand Diels–Alder reaction between electron-deficient tetrazine and strained trans-cyclooctene (TCO) derivatives. This reaction has been heavily utilized in recent studies due to its remarkably fast reaction kinetics and *in vitro* selectivity.[92,94] For example, Rossin *et al.* reported for the first time the use of the click reaction between tetrazine and a TCO-tagged antibody in an *in vivo* tumor model.[93] [111]In labeled tetrazine-DOTA construct was used for the *in vivo* reaction with a TCO anti-tumor-associated glycoprotein 72 (TCO-anti-TAG72)

monoclonal antibody. Multi-step SPECT/CT images in mice bearing colon cancer xenografts showed localization of the radioactivity in the tumour with minimal background (Figure 33).
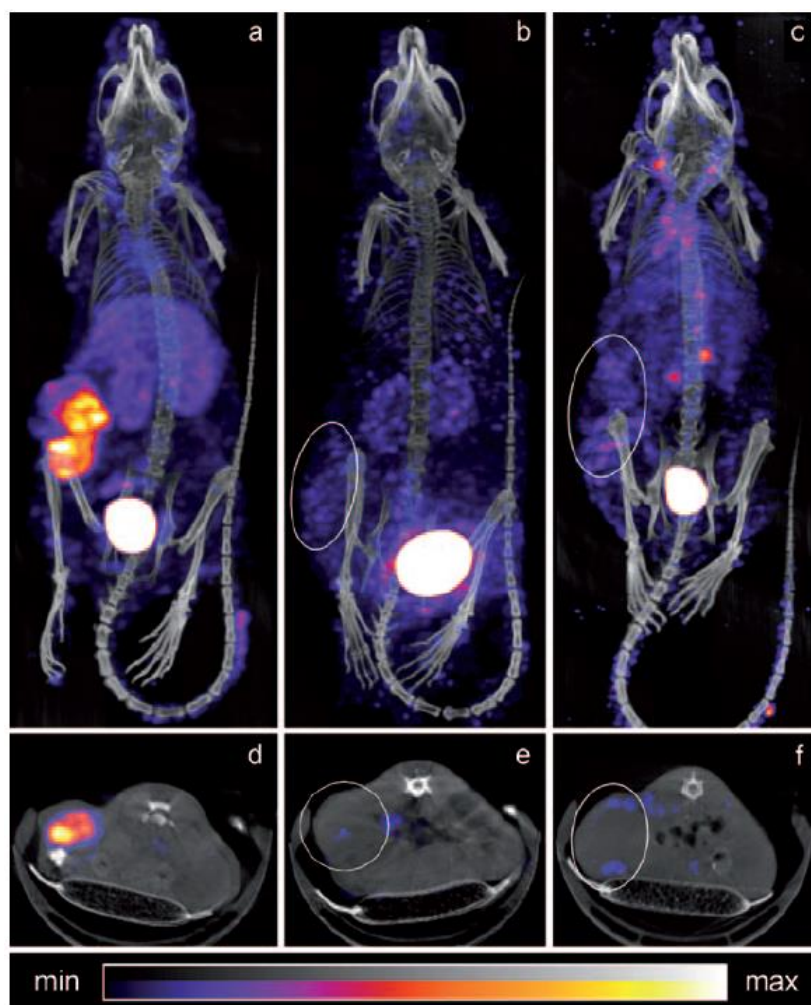
Figure 33 SPECT/CT images of mice bearing colon cancer xenografts: posterior projections of mice preinjected with a) 42 MBq[111]In labeled tetrazine-DOTA administered 24 h after the TCO-anti-TAG72 antibody injection, b) 20MBq[111]In-labeled tetrazine-DOTA administered 24 h after anti-TAG72 antibody injection, and c) 50 MBq[111]In-labeled tetrazine-DOTA administered 24 h after a TCO-modified rituximab lacking specificity for TAG72 was preinjected; d)–f) single transverse slices (2 mm) passing through the tumors in (a)–(c). (Reprinted with permission of [93])

In our group, a novel pre-targeted approach combining targeted US imaging and bioorthogonal chemistry was developed.[95] As a proof-of-concept, the reactivity of

tetrazine-tagged MBs (MB$_{Tz}$) towards TCO-conjugated anti-VEGFR2 antibody was evaluated in VEGFR2positive H520 cells. Streptavidin-coated MBs were functionalized with a biotinylated tetrazine as part of the evaluation of the capturing strategy. In order to validate the ligation reaction, the biotinylated tetrazine was initially tested in an *in vitro* fluorescence assay in H520 cells tagged with TCO–anti-VEGFR2 and results indicated identical intensity when compared to a commercially available biotinylated anti-VEGFR2 antibody (biotin–antiVEGFR2) with minimal non specific binding in the negative controls.

A flow assay was conducted subsequently to test the ability of the approach to localize MB$_{Tz}$ at the target in a dynamic system. A semi-quantitative analysis was performed by comparing the area covered by the MBs in each image to the area covered by the cells. Results showed that MB$_{Tz}$ binding to TCO–antiVEGFR2 tagged H520 cells was an order of magnitude higher than that of untagged cells. A preliminary study in animal models was conducted and US imaging was performed using CD1 nu/nu mice bearing SKOV-3 human adenocarcinoma tumours. Images showed high retention of MB$_{Tz}$ in vascularized regions of the tumors (Figure 34).
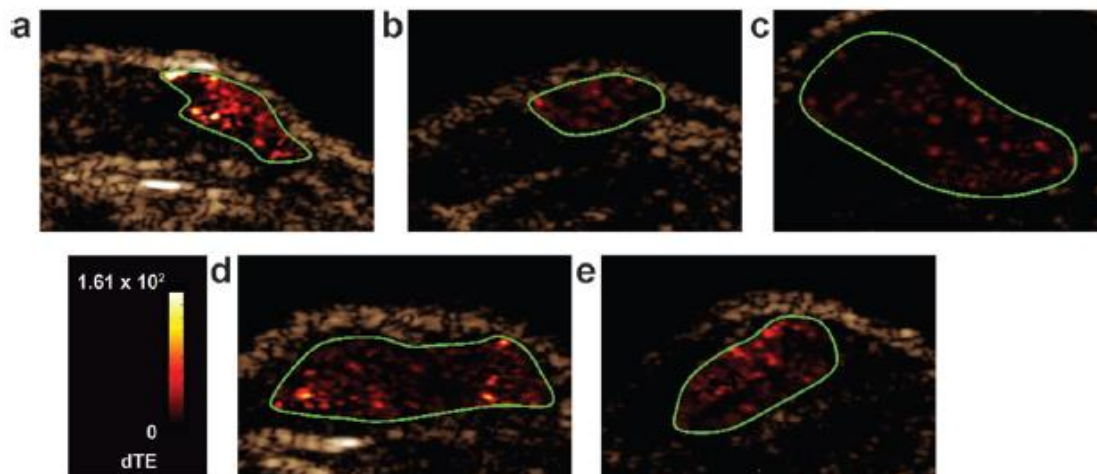
Figure 34 Transverse color-coded parametric nonlinear contrast mode US images acquired 4 min after intravenous administration of MB_{Tz} to: a) SKOV-3 human adenocarcinoma murine tumor model (VEGFR2(+)) pre-administered with TCO–antiVEGFR2; and b) the same model without antibody; c) A431 human epidermoidcarcinoma tumor (VEGFR2(-)) pre-administered with TCO–antiVEGFR2. Images of SKOV-3 murine tumor models following administration of d) VEGFR2-targeted MBs (MBV); and e) Control MBs (MBC) with pre-administered TCO–antiVEGFR2. Regions of interest were based on the vascularity of the tumors determined from the initial distribution of the MBs following injection. dTE = differential targeted enhancement. (Reprinted with permission of [95])

4.6. Objective

The objective was to combine the benefits of US imaging and the bioorthogonal chemistry that takes place between tetrazine functionalized MBs and TCO modified antibodies to create a new breast cancer molecular imaging technology. The focus is to create a MB that can selectively bind to uPAR such that the probe could eventually be used to evaluate protease receptor expression levels and hence the aggressiveness and metastatic potential of breast cancers using US.

The initial goal involved the preparation of a TCO modified antibody that can bind uPAR followed by *in vitro* testing of the bioorthogonal reaction between tetrazine-coated MBs and TCO-conjugated anti-uPAR antibodies. Work was done in a flow chamber system, as opposed to simply in culture, to mimic conditions found *in vivo*. Success would ultimately lead to US imaging studies in small animal models.

4.7. Results

4.7.1. TCO anti-uPAR antibody conjugation

The TCO-conjugated antibody (TCO–anti-uPAR) was prepared by combining an excess (20 equivalents) of commercially available (E)-cyclooct-4-enyl-2,5-dioxopyrrolidin-1-yl carbonate (TCO–NHS) with a murine monoclonal antibody, subclass IgG_{2a} recognizing the human urokinase plasminogen activator receptor (uPAR) (American Diagnostica Inc., Product No. 3936) at 4 °C overnight (Scheme 11). The reaction was conducted in PBS where the pH was adjusted to 8.5–9.0 using 1 M Na_2CO_3. After purification using a 30 kDa centrifugal filter (Amicon Ultra-0.5) MALDI-TOFMS showed an average of 2.7 TCO groups per antibody in the product (Figure 35).

| TCO-NHS | Anti-uPAR antibody | TCO-uPAR antibody |
| 20 Equivalents | 1 Equivalent | |
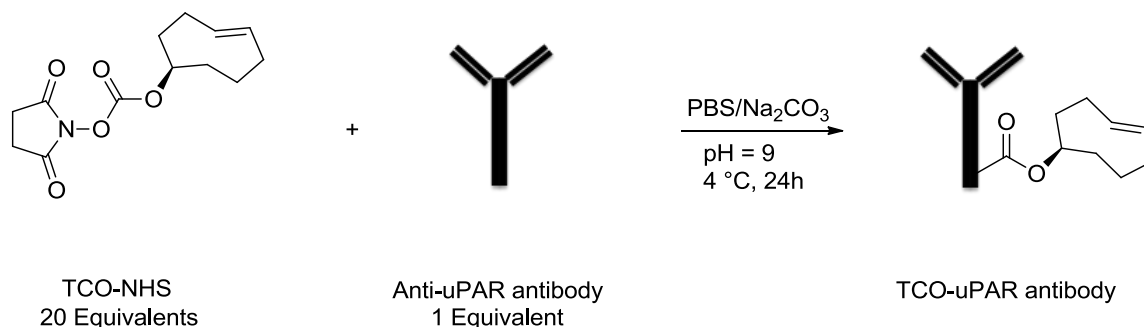
Scheme 11 Conjugation of TCO with anti-uPAR antibody.
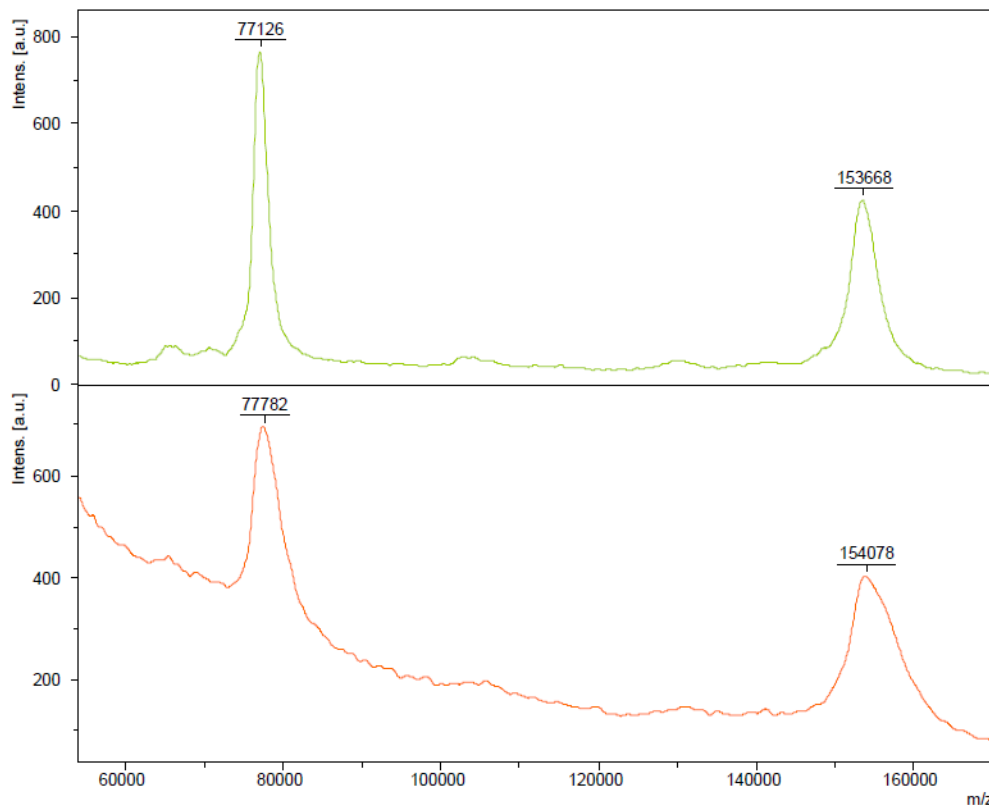
Figure 35 MALDI-TOF analysis of unconjugated anti-uPAR antibody (top) and TCO-anti-uPAR (bottom). In ultra-high mass spectrometry, as in this case, typically the resolution is lower. The samples shown in this spectra did not ionize well (as evidenced in the low intensity), which may be due to other salts and contaminants in solution which suppress ionization. This causes the peaks to widen as well. However, there is a large enough shift between the two spectra that it signifies a different protein.[96]

4.7.2. uPAR Binding Assay

Before conducting the flow experiment, it was important to show that the addition of the TCO group did not reduce the affinity of the parent antibody for the target. A preliminary fluorescence intensity experiment was conducted in which the ability of the biotinylated tetrazine (Figure 36) (obtained from Aimen Zlitni) to react with uPAR expressing MDA-MB-231 cells tagged with the TCO modified antibody was tested. The biotinylated tetrazine was added to MDAMB-231 cells that had been incubated with the antibody (TCO+) and cells that lacked the antibody (TCO-) and the extent of tetrazine–

TCO conjugation was determined by adding a FITC-labeled anti-biotin antibody (FITC-antiBiotin) and measuring the arising fluorescence in cell lysates. Results indicated a 4-fold increase in fluorescence intensity in the (TCO+) cells (Figure 37) compared to that observed when no TCO was present.
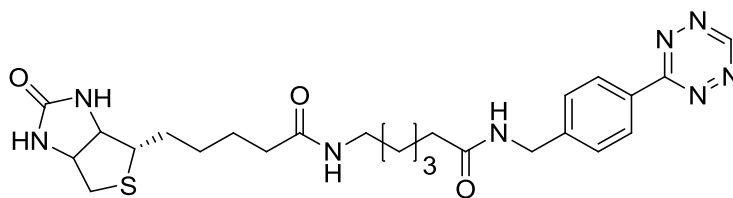
Figure 36 Chemical structure of biotinylated tetrazine; *N*-(4-(1,2,4,5-tetrazin-3-yl)benzyl)-6-(5-((4*S*)-2-oxohexahydro-1*H*-thieno[3,4-*d*]imidazol-4-yl)pentanamido)hexanamide.
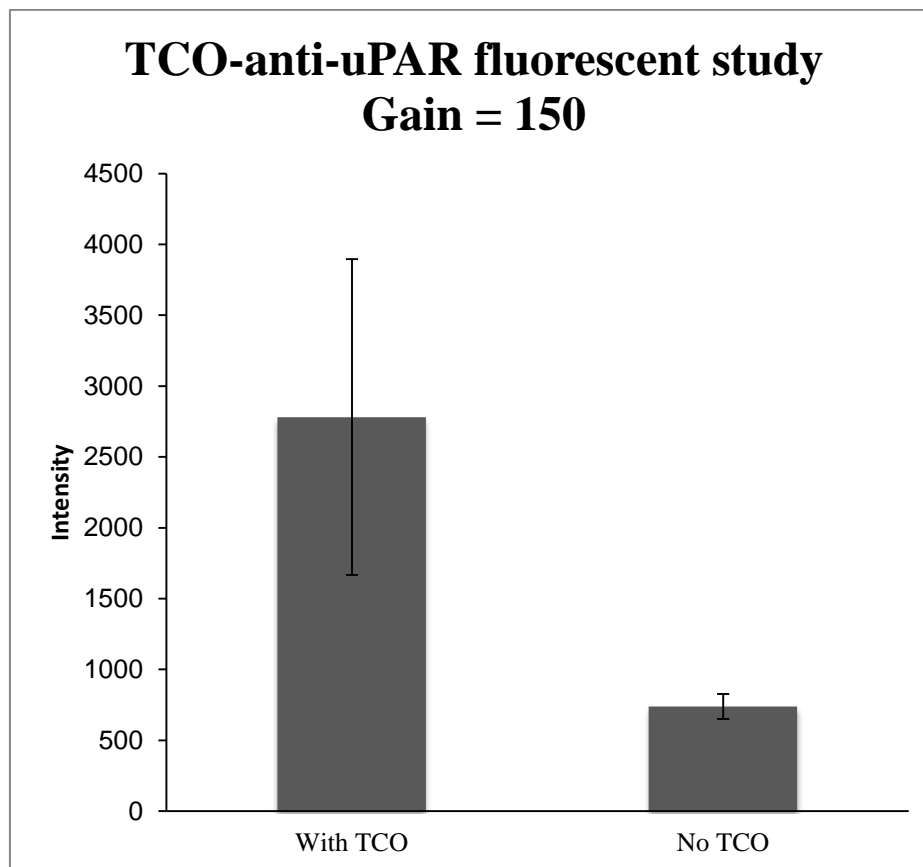
Figure 37 uPAR fluorescence intensity study for the binding of FITC-antiBiotin with biotinylated tetrazine in the presence (left) and absence (right) of TCO on MDA-MB-231 cells.

4.7.3. Flow Chamber Cell Adhesion Assay

A novel *in vitro* flow assay that has previously been developed in our group was used to evaluate the effectiveness of the MB_{Tz} in capturing the TCO-anti-uPAR. MBs were tested under flow conditions that mimic rheology properties in tumor capillaries by using a parallel-plate flow chamber system (Glycotech, Rockville, Md.). Initially, a preliminary study using uPAR- expressing MDA-MB-231 cells was conducted in which cells were incubated at room temperature with TCO–anti-uPAR for 30 minutes prior to the assay (TCO +). Cells were washed with PBS for 2 minutes using a syringe pump to remove any unbound antibody, followed by either functionalized (MB_{Tz}) or unmodified

MBs. The procedure was performed over 4 minutes at a 100 s^{-1} shear rate to mimic flow conditions found *in vivo* and to allow for comparison to our previous work involving VEGFR2 targeted MBs. After 4 min, cells were washed with PBS for 2 minutes at a 1000 s^{-1} shear rate in order to eliminate MBs that were simply sticking to the well through nonspecific binding interactions. Plates were visualized using an optical microscope and videos were taken during the flow assay and static images for analysis acquired after the final washing step was completed (Figure 38).

Analysis of the results of the flow experiment indicated that the MB_{Tz} concentrated to a significant extent on MDA-MB-231 cells (TCO+) when compared to the controls (TCO-) (Figure 38). A semi-quantitative analysis was performed by comparing the area covered by the MBs in each image to the area covered by the cells determined using an open-source image processing package. Although results indicated higher binding to the (TCO+) cells, the total number of bubbles bound per cell was less than that which has been previously reported for VEGFR2. This could be attributed to the difference in expression levels of the targets (uPAR vs. VEGFR2). One other related observation was that the total number of cells per well decreased significantly after the washing steps due to the modest adhesion properties of the MDA-MB-231 cells.
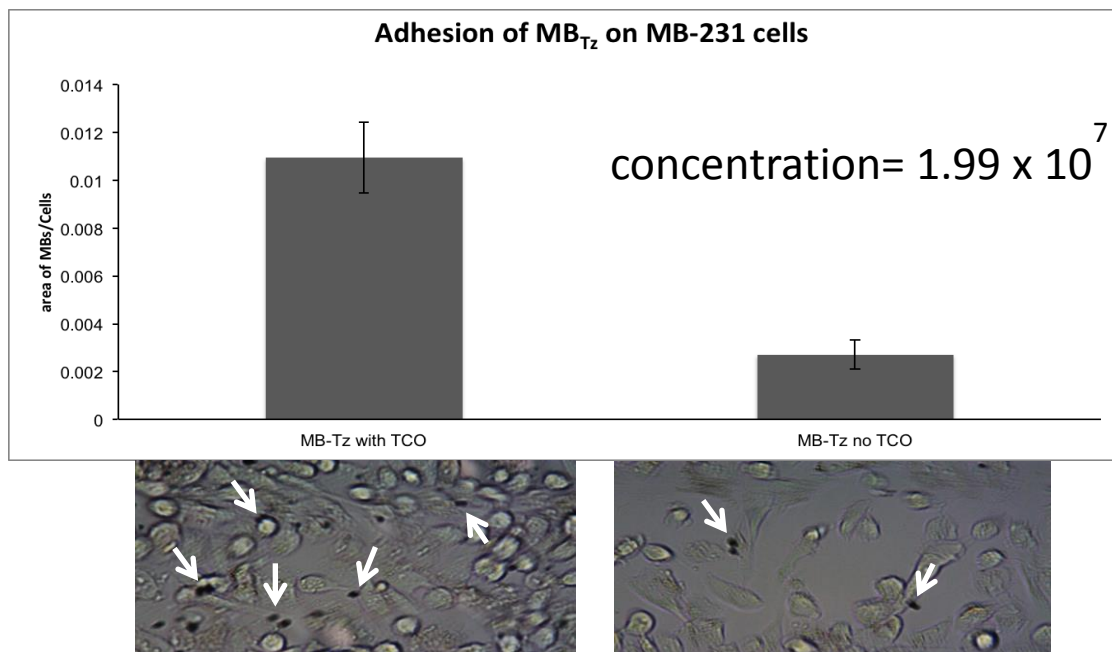
Figure 38 Graphical analysis of the number of MBs bound per cell based on relative area from the flow chamber adhesion assay following washing. The two bright-field microscopy images are shown; one image from one well of both MB-Tz with TCO (left) and MB-Tz with no TCO (right). The MBs appear as black spheres (with select examples highlighted by the white arrows).

To address the adherence issue, anA431 cell line was used as it is known to overexpress uPAR, is sufficiently adherent and it has been used successfully in prior flow experiments. The flow assay was repeated with all controls, each sample done in duplicate, using A431 cells as the uPAR expressing cell line (uPAR +) and MCF7 as a negative control (uPAR -).[97] In order to test the difference between pre-targeted (capture strategy) and conventional targeting, MB$_{Tz}$ was pre-incubated with TCO-anti-uPAR antibodies (MB$_{uPAR}$) to generate an actively targeted construct. Results of the experiment showed minimal binding in all of the negative controls; MCF7 cells incubated with the antibody, A431 cells exposed to MB$_{Tz}$ without antibody treatment and antibody treated A431 cells exposed to control MBs lacking the tetrazine moiety (MB$_c$). The binding of the MB$_{Tz}$ to A431 (TCO+) cells was 6 fold higher than the highest negative control and a

qualitative assessment of the images and videos indicates a significantly higher binding than the negative controls. No significant difference between the pre-targeted MB_{Tz} and the MB_{uPAR} was observed. It is worth mentioning that a similar pattern was observed when repeating the experiment with the same controls on a different day, where graphical analysis of both experiments (Figure 39 and Figure 40) and a representative of the microscopic images (Figure 41) are shown below.
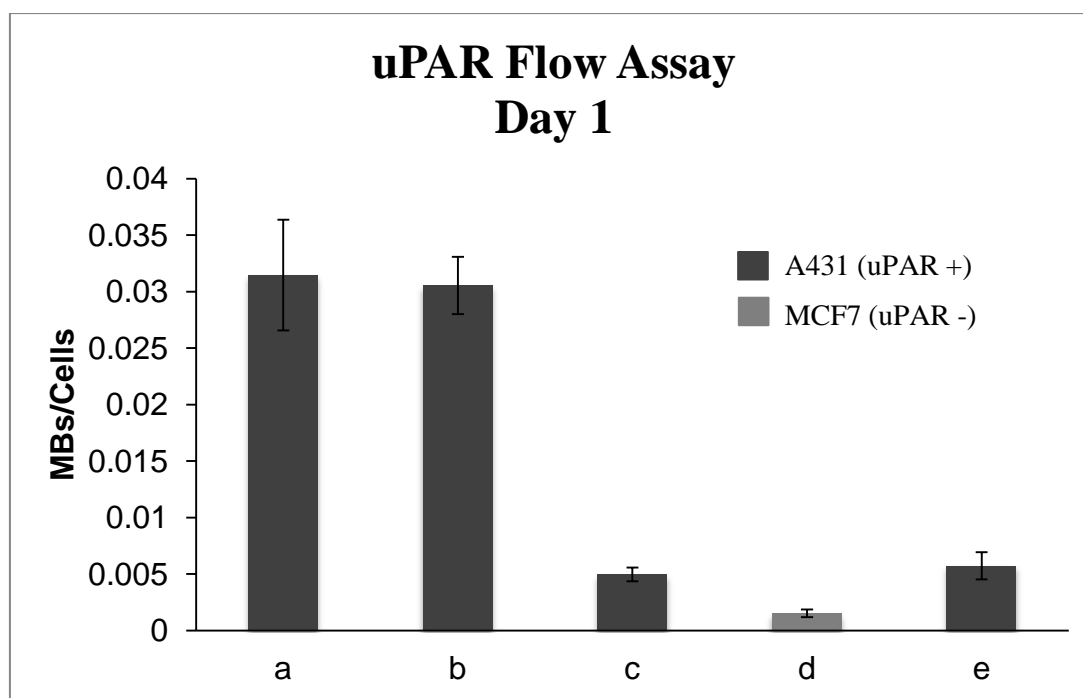
Figure 39 Graphical analysis of the number of MBs bound per cell based on relative area from the flow chamber adhesion assay following washing on day one, where a=TCO-anti-uPAR + MB_{Tz}, b=MB_{uPAR}, c=MB_{Tz}, d=TCO-anti-uPAR + MB_{Tz} and e=TCO-anti-uPAR + MB_C (n=2).
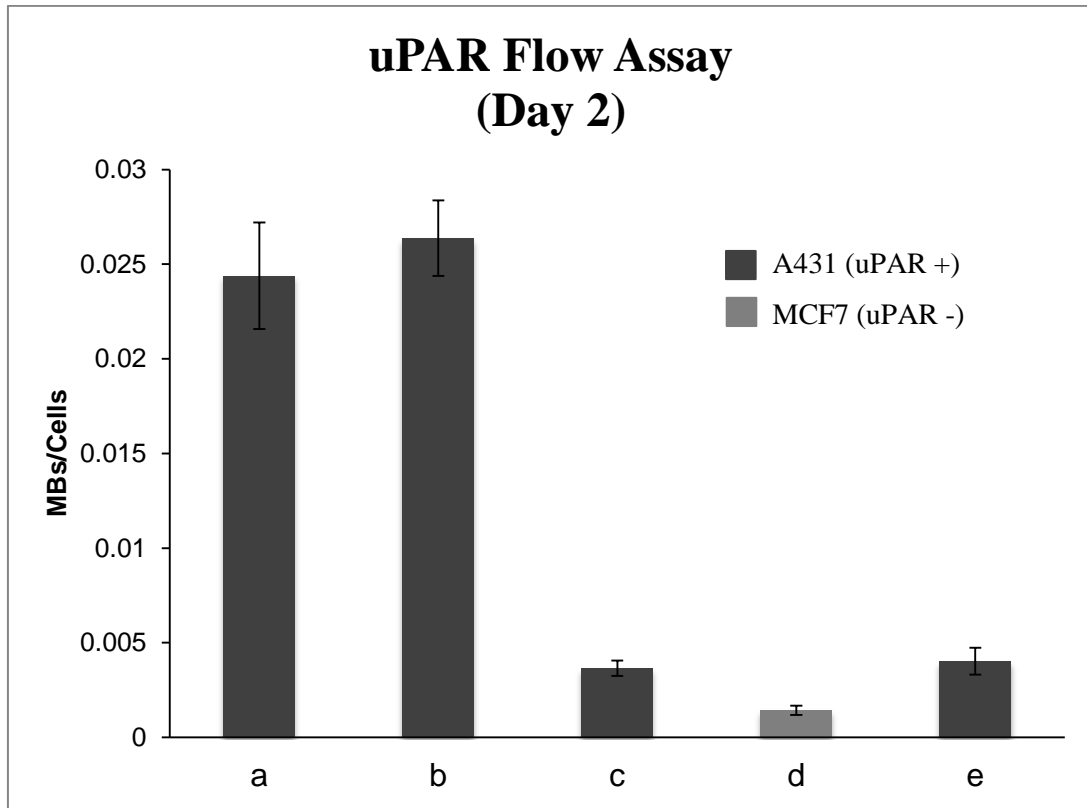
Figure 40 Graphical analysis of the number of MBs bound per cell based on relative area from the flow chamber adhesion assay following washing on day two, where a=TCO-anti-uPAR + MB_{Tz}, b=MB_{uPAR}, c=MB_{Tz}, d=TCO-anti-uPAR + MB_{Tz} and e=TCO-anti-uPAR + MB_C (n=2).
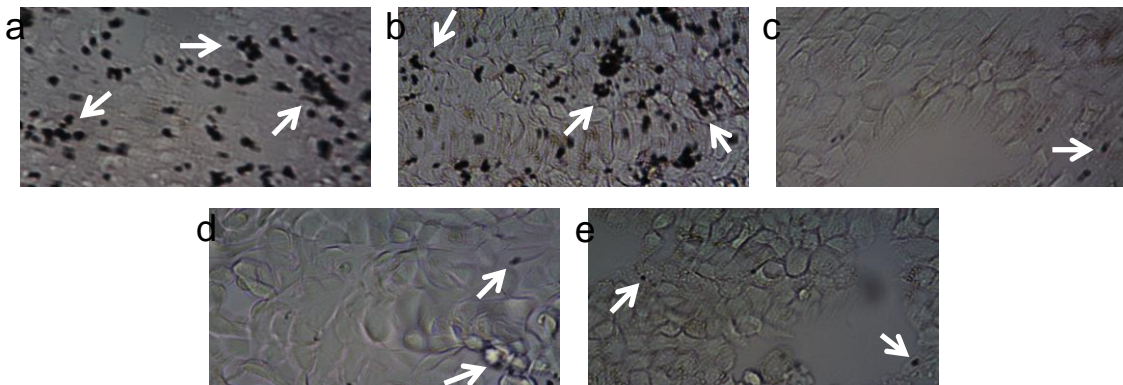
Figure 41 Bright-field microscopy images showing binding of: a) A431 cells + TCO-anti-uPAR + MB_{Tz}, b)A431 cells + MB_{Tz}-TCO-anti-uPAR, c) A431 cells + MB_{Tz}, d) MCF7 cells + TCO-anti-uPAR + MB_{Tz} and e) A431 cells + TCO-anti-uPAR + MB_C. The MBs appear as black spheres with select examples highlighted by the white arrows.

4.8. Summary and Future Work

TCO was successfully conjugated to the anti-uPAR antibody and fluorescence experiments in MDA-MB-231 cells validated the selective reactivity of the TCO-anti-uPAR antibody towards a biotinylated tetrazine derivative. Also, uPAR expressing A431 cells were incubated with the antibody and tested in a flow assay where they were able to capture the MB_{Tz} selectively. Next steps for this work should involve *in vivo* US imaging in animal xenograft models. The antibody will be injected first, allowed to accumulate in tumours and subsequently clear from the rest of the body. After this, the MB_{Tz} will be injected and US will be taken to assess the contrast enhancement achieved by the MBs.

CHAPTER FIVE: CONCLUSION AND FUTURE WORK

The work described in this thesis was divided into two parts. The first component was done to create a MI probe that could target increased IR expression in different types of cancer, with particular focus on breast cancer. In the attempts to design such a probe, we have been able to selectively conjugate halogenated prosthetic groups to insulin at the B29-Lys position and successfully produce the ^{18}F-analogue which showed adequate stability in saline and PBS. The lead compound, (**4**), also showed affinity for the IR comparable to insulin. Further development of the probe was halted because of concerns over metabolic stability of the vector and target localization issues that arose when testing the similar B1 probe *in vivo.* Future efforts on the IR probe should focus on further enhancement of metabolic stability or switching to a different strategy using antibodies targeting IGF-1 or IR.

An antibody-targeted US imaging approach targeting uPAR was investigated as another avenue to preparing MI probes for breast cancer. The flow experiments were successful and showed that the pre-targeted approach using MBs can be used to detect uPAR *in vitro*. This was evident by the ability of uPAR-expressing cells in capturing the MB$_{Tz}$ once the cells were incubated with the TCO-conjugated antibody. Short term goals for this work should include *in vivo* US imaging in animal xenograft model expressing uPAR.

Although preliminary data proves promising, there are two potential limitations with this strategy. First, endogenous uPA is overexpressed concurrently with overexpression of uPAR. This can be overcome using antibodies that bind uPAR whether

or not uPA is present. Also, this platform was based upon a streptavidin-biotin interaction at the MB surface, which is known to cause an adverse reaction in humans.[98] The long term objective should therefore be to design the next generation of tetrazine-bubbles that are human compatible. This is currently an active area of research within the group.

REFERENCES

(1)   Canadian Cancer Society's Advisory Committee on Cancer Statistics. Canadian Cancer Statistics 2014. Toronto, ON: Canadian Cancer Society; **2014**.

(2)   Hutchinson, L. *Nat. Rev. Clin. Oncol.* **2010**, *7*, 669–670.

(3)   Leitch, a M.; Dodd, G. D.; Costanza, M.; Linver, M.; Pressman, P.; McGinnis, L.; Smith, R. a. *CA. Cancer J. Clin.* **1997**, *47*, 150–153.

(4)   Smith, R. a; Cokkinides, V.; Eyre, H. J. *CA. Cancer J. Clin.* **2002**, *56*, 11–25; quiz 49–50.

(5)   Valliant, J. F. *J. Nucl. Med.* **2010**, *51*, 1258–1268.

(6)   Hruska, C. B.; Boughey, J. C.; Phillips, S. W.; Rhodes, D. J.; Wahner-Roedler, D. L.; Whaley, D. H.; Degnim, A. C.; O'Connor, M. K. *Am. J. Surg.* **2008**, *196*, 470–476.

(7)   Taubes, G. *Science* **2012**, *335*, 28, 30–32.

(8)   Ohinmaa, A.; Jacobs, P.; Pharmd, S. S.; Johnson, J. A. *Can. J. Diabetes* **2004**, *28*, 1–8.

(9)   Hossain, P.; Kawar, B.; El Nahas, M. *N. Engl. J. Med.* **2007**, *356*, 213–215.

(10)   Kahn, S. E.; Hull, R. L.; Utzschneider, K. M. *Nature* **2006**, *444*, 840–846.

(11)   Monami, M.; Lamanna, C.; Pala, L.; Bardini, G.; Cresci, B.; Francesconi, P.; Balzi, D.; Marchionni, N.; Rotella, C. M.; Mannucci, E. *Exp. Clin. Endocrinol. Diabetes* **2008**, *116*, 184–189.

(12)   Goodwin, P. J.; Ligibel, J. a; Stambolic, V. *J. Clin. Oncol.* **2009**, *27*, 3271–3273.

(13)   Calle, E. E.; Rodriguez, C.; Walker-Thurmond, K.; Thun, M. J. *N. Engl. J. Med.* **2003**, *348*, 1625–1638.

(14)   Renehan, A. G.; Frystyk, J.; Flyvbjerg, A. *Trends Endocrinol. Metab.* **2006**, *17*, 328–336.

(15)   Mayer, J. P.; Zhang, F.; Dimarchi, R. D. *Biopolymers* **2007**, *88*, 687–713.

(16) Chow, L. S.; Albright, R. C.; Bigelow, M. L.; Toffolo, G.; Cobelli, C.; Nair, K. S. *Am. J. Physiol. Endocrinol. Metab.* **2006**, *291*, 729–736.

(17) Nakae, J.; Kido, Y.; Accili, D. *Endocr. Rev.* **2001**, *22*, 818–835.

(18) Boyd, D. B. *Integr. Cancer Ther.* **2003**, *2*, 315–329.

(19) Frasca, F.; Pandini, G.; Sciacca, L.; Pezzino, V.; Squatrito, S.; Belfiore, A.; Vigneri, R. *Arch. Physiol. Biochem.* **2008**, *114*, 23–37.

(20) Frittitta, L.; Cerrato, a; Sacco, M. G.; Weidner, N.; Goldfine, I. D.; Vigneri, R. *Breast Cancer Res. Treat.* **1997**, *45*, 141–147.

(21) Cox, M. E.; Gleave, M. E.; Zakikhani, M.; Bell, R. H.; Piura, E.; Vickers, E.; Cunningham, M.; Larsson, O.; Fazli, L.; Pollak, M. *Prostate* **2009**, *69*, 33–40.

(22) Huang, J.; Morehouse, C.; Streicher, K.; Higgs, B. W.; Gao, J.; Czapiga, M.; Boutrin, A.; Zhu, W.; Brohawn, P.; Chang, Y.; Viner, J.; LaVallee, T.; Richman, L.; Jallal, B.; Yao, Y. *PLoS One* **2011**, *6*, e26177.

(23) Frasca, F.; Pandini, G.; Scalia, P.; Sciacca, L.; Mineo, R.; Costantino, a; Goldfine, I. D.; Belfiore, a; Vigneri, R. *Mol. Cell. Biol.* **1999**, *19*, 3278–3288.

(24) Papa, V.; Pezzino, V.; Costantino, a; Belfiore, a; Giuffrida, D.; Frittitta, L.; Vannelli, G. B.; Brand, R.; Goldfine, I. D.; Vigneri, R. *J. Clin. Invest.* **1990**, *86*, 1503–1510.

(25) Min, Y.; Adachi, Y.; Yamamoto, H.; Ito, H.; Itoh, F. *Cancer Res.* **2003**, *63*, 6432–6441.

(26) Buck, E.; Mulvihill, M. *Expert Opin. Investig. Drugs* **2011**, *20*, 605–621.

(27) Bähr, C.; Groner, B. *Growth Horm. IGF Res.* **2004**, *14*, 287–295.

(28) Weroha, S.; Haluska, P. *J. Mammary Gland Biol. Neoplasia* **2008**, *13*, 471–483.

(29) Wester, H.-J. *Clin. Cancer Res.* **2007**, *13*, 3470–3481.

(30) Pennant, M.; Takwoingi, Y.; Pennant, L.; Davenport, C.; Fry-Smith, A.; Eisinga, A.; Andronis, L.; Arvanitis, T.; Deeks, J.; Hyde, C. *Health Technol. Assess. (Rockv).* **2010**, *14*, 1–103.

(31) Mariani, G.; Bruselli, L.; Kuwert, T.; Kim, E. E.; Flotats, A.; Israel, O.; Dondi, M.; Watanabe, N. *Eur. J. Nucl. Med. Mol. Imaging* **2010**, *37*, 1959–1985.

(32) Gözde Özkan, Z.; Kuyumcu, S.; Balköse, D.; Ozkan, B.; Aksakal, N.; Yılmaz, E.; Sanlı, Y. *Mol. Imaging Radionucl. Ther.* **2013**, *22*, 49–55.

(33) Koopmans, K. P.; Glaudemans, a W. J. M. *Eur. J. Nucl. Med. Mol. Imaging* **2012**, *39 Suppl 1*, S4–10.

(34) Linde, S.; Hansen, B.; Sonne, O.; Holst, J. J.; Gliemann, J. *Diabetes* **1981**, *30*, 1–8.

(35) Guenther, K. J.; Yoganathan, S.; Garofalo, R.; Kawabata, T.; Strack, T.; Labiris, R.; Dolovich, M.; Chirakal, R.; Valliant, J. F. *J. Med. Chem.* **2006**, *49*, 1466–1474.

(36) Kurtaran, A.; Li, S. R.; Raderer, M.; Leimer, M.; Müller, C.; Pidlich, J.; Neuhold, N.; Hübsch, P.; Angelberger, P.; Scheithauer, W. *J. Nucl. Med.* **1995**, *36*, 1875–1881.

(37) Iozzo, P.; Osman, S.; Glaser, M.; Knickmeier, M.; Ferrannini, E.; Pike, V. W.; Camici, P. G.; Law, M. P. *Nucl. Med. Biol.* **2002**, *29*, 73–82.

(38) Glaser, M.; Brown, D. J.; Law, M. P.; Iozzo, P.; Waters, S. L.; Poole, K.; Knickmeier, M.; Camici, P. G.; Pike, V. W. *J. Label. Compd. Radiopharm.* **2001**, *44*, 465–480.

(39) Jalilian, a. R.; Garousi, J.; Akhlaghi, M.; Rowshanfarzad, P. *J. Radioanal. Nucl. Chem.* **2009**, *279*, 791–796.

(40) Gholami, E.; Akhlaghi, M.; Bolourinovin, F.; Rajabifar, S. *Nukleonika* **2007**, *52*, 145–151.

(41) Kamei, N.; Morishita, M.; Kanayama, Y.; Hasegawa, K.; Nishimura, M.; Hayashinaka, E.; Wada, Y.; Watanabe, Y.; Takayama, K. *J. Control. Release* **2010**, *146*, 16–22.

(42) Sundararajan, C.; Besanger, T. R.; Labiris, R.; Guenther, K. J.; Strack, T.; Garafalo, R.; Kawabata, T. T.; Finco-Kent, D.; Zubieta, J.; Babich, J. W.; Valliant, J. F. *J. Med. Chem.* **2010**, *53*, 2612–2621.

(43) Shai, Y.; Kirk, K. L.; Channing, M. A.; Dunn, B. B.; Lesniak, M. A.; Eastman, R. C.; Finn, R. D.; Roth, J.; Jacobson, K. A. *Biochemistry* **1989**, *28*, 4801–4806.

(44) Eastman, R.; Carson, R.; Jacobson, K. *Diabetes* **1992**, *41*, 855–860.

(45) Simms, R. W.; Kim, D. H.; Weaver, D. M.; Sundararajan, C.; Blacker, M.; Stephenson, K. A; Valliant, J. F. *Chemistry* **2012**, *18*, 6746–6749.

(46)   Kim, D. H.; Blacker, M.; Valliant, J. F. *J. Med. Chem.* **2014**, *57*, 3678–3686.

(47)   Kavimandan, N.; Losi, E. *Bioconjug. Chem.* **2006**, *17*, 1376–1384.

(48)   Myers, S. R.; Yakubu-Madus, F. E.; Johnson, W. T.; Baker, J. E.; Cusick, T. S.; Williams, V. K.; Tinsley, F. C.; Kriauciunas, A.; Manetta, J.; Chen, V. J. *Diabetes* **1997**, *46*, 637–642.

(49)   Petrus, A. K.; Vortherms, A. R.; Fairchild, T. J.; Doyle, R. P. *ChemMedChem* **2007**, *2*, 1717–1721.

(50)   Petrus, A. K.; Allis, D. G.; Smith, R. P.; Fairchild, T. J.; Doyle, R. P. *ChemMedChem* **2009**, *4*, 421–426.

(51)   Hinds, K. D.; Kim, S. W. *Adv. Drug Deliv. Rev.* **2002**, *54*, 505–530.

(52)   Lee, S.; Kim, K.; Kumar, T. S.; Lee, J.; Kim, S. K.; Lee, D. Y.; Lee, Y.; Byun, Y. *Bioconjug. Chem.* **2005**, *16*, 615–620.

(53)   Vaidyanathan, G.; Zalutsky, M. R. *Int. J. Rad. Appl. Instrum. B.* **1992**, *19*, 275–281.

(54)   Vaidyanathan, G.; Zalutsky, M. R. *Bioconjug. Chem.* **1994**, *5*, 352–356.

(55)   Jahan, M.; Nag, S.; Krasikova, R.; Weber, U.; Muhs, A.; Pfeifer, A.; Spenger, C.; Willbold, D.; Gulyás, B.; Halldin, C. *Nucl. Med. Biol.* **2012**, *39*, 315–323.

(56)   Liu, F.; Kohn, W. D.; Mayer, J. P. *J. Pept. Sci.* **2012**, *18*, 336–341.

(57)   Milazzo, G.; Giorgino, F.; Damante, G. *Cancer Res.* **1992**, 3924–3930.

(58)   Duckworth, W. C.; Bennett, R. G.; Hamel, F. G. *Endocr. Rev.* **1998**, *19*, 608–624.

(59)   Kurtzhals, P.; Havelund, S.; Jonassen, I.; Kiehr, B.; Larsen, U. D.; Ribel, U.; Markussen, J. *Biochem. J.* **1995**, *312 (Pt 3*, 725–731.

(60)   Sharkey, R. M.; Behr, T. M.; Mattes, M. J.; Stein, R.; Griffiths, G. L.; Shih, L. B.; Hansen, H. J.; Blumenthal, R. D.; Dunn, R. M.; Juweid, M. E.; Goldenberg, D. M. *Cancer Immunol. Immunother.* **1997**, *44*, 179–188.

(61)   Greguric, I.; Taylor, S. R.; Denoyer, D.; Ballantyne, P.; Berghofer, P.; Roselt, P.; Pham, T. Q.; Mattner, F.; Bourdier, T.; Neels, O. C.; Dorow, D. S.; Loc'h, C.; Hicks, R. J.; Katsifis, A. *J. Med. Chem.* **2009**, *52*, 5299–5302.

(62) Olberg, D. E.; Arukwe, J. M.; Grace, D.; Hjelstuen, O. K.; Solbakken, M.; Kindberg, G. M.; Cuthbertson, A. *J. Med. Chem.* **2010**, *53*, 1732–1740.

(63) Yamaguchi, Y.; Flier, J. S.; Yokota, A.; Benecke, H.; Backer, J. M.; Moller, D. E. *Endocrinology* **1991**, *129*, 2058–2066.

(64) Del Vecchio, S.; Stoppelli, M. P.; Carriero, M. V; Fonti, R.; Massa, O.; Li, P. Y.; Botti, G.; Cerra, M.; D'Aiuto, G.; Esposito, G. *Cancer Res.* **1993**, *53*, 3198–3206.

(65) Ploug, M.; Ellis, V. *FEBS Lett.* **1994**, *349*, 163–168.

(66) Noh, H.; Hong, S.; Huang, S. *Theranostics* **2013**, *3*, 487–495.

(67) Solberg, H.; Ploug, M.; Hoyer-Hansen, G.; Nielsen, B. S.; Lund, L. R. *J. Histochem. Cytochem.* **2001**, *49*, 237–246.

(68) Wei, C.; Möller, C. C.; Altintas, M. M.; Li, J.; Schwarz, K.; Zacchigna, S.; Xie, L.; Henger, A.; Schmid, H.; Rastaldi, M. P.; Cowan, P.; Kretzler, M.; Parrilla, R.; Bendayan, M.; Gupta, V.; Nikolic, B.; Kalluri, R.; Carmeliet, P.; Mundel, P.; Reiser, J. *Nat. Med.* **2008**, *14*, 55–63.

(69) Beschorner, R.; Schluesener, H. J.; Nguyen, T. D.; Magdolen, V.; Luther, T.; Pedal, I.; Mattern, R.; Meyermann, R.; Schwab, J. M. *Neuropathol. Appl. Neurobiol.* **2000**, *26*, 522–527.

(70) Smith, H. W.; Marshall, C. J. *Nat. Rev. Mol. Cell Biol.* **2010**, *11*, 23–36.

(71) De Bock, C. E.; Wang, Y. *Med. Res. Rev.* **2004**, *24*, 13–39.

(72) Nielsen, B. S.; Rank, F.; Illemann, M.; Lund, L. R.; Danø, K. *Int. J. Cancer* **2007**, *120*, 2086–2095.

(73) Alpízar-Alpízar, W.; Nielsen, B. S.; Sierra, R.; Illemann, M.; Ramírez, J. A.; Arias, A.; Durán, S.; Skarstein, A.; Ovrebo, K.; Lund, L. R.; Laerum, O. D. *Int. J. Cancer* **2010**, *126*, 405–415.

(74) Kotzsch, M.; Dorn, J.; Doetzer, K.; Schmalfeldt, B.; Krol, J.; Baretton, G.; Kiechle, M.; Schmitt, M.; Magdolen, V. *Biol. Chem.* **2011**, *392*, 1047–1051.

(75) Giannopoulou, I.; Mylona, E.; Kapranou, a.; Mavrommatis, J.; Markaki, S.; Zoumbouli, C.; Keramopoulos, a.; Nakopoulou, L. *Cancer Lett.* **2007**, *246*, 262–267.

(76)   Ellis, V.; Pyke, C.; Eriksen, J.; Solberg, H.; Danø, K. *Ann. N. Y. Acad. Sci.* **1992**, *667*, 13–31.

(77)   Dullin, C.; Zientkowska, M.; Napp, J.; Missbach-Guentner, J.; Krell, H.-W.; Müller, F.; Grabbe, E.; Tietze, L.-F.; Alves, F. *Mol. Imaging* **2009**, *8*, 2–14.

(78)   Yang, L.; Peng, X.-H.; Wang, Y. A.; Wang, X.; Cao, Z.; Ni, C.; Karna, P.; Zhang, X.; Wood, W. C.; Gao, X.; Nie, S.; Mao, H. *Clin. Cancer Res.* **2009**, *15*, 4722–4732.

(79)   Liu, D.; Overbey, D.; Watkinson, L.; Giblin, M. F. *Bioconjug. Chem.* **2009**, *20*, 888–894.

(80)   Li, Z.-B.; Niu, G.; Wang, H.; He, L.; Yang, L.; Ploug, M.; Chen, X. *Clin. Cancer Res.* **2008**, *14*, 4758–4766.

(81)   Persson, M.; Madsen, J.; Østergaard, S.; Jensen, M. M.; Jørgensen, J. T.; Juhl, K.; Lehmann, C.; Ploug, M.; Kjaer, A. *J. Nucl. Med.* **2012**, *53*, 138–145.

(82) Dorthe Skovgaard; Rigshospitalet, Denmark. Evaluation of a New Radiotracer (^{64}Cu-DOTA-AE105) for Diagnosing Aggressive Cancer With Positron Emission Tomography. In: ClinicalTrials.gov [Internet]. Bethesda (MD): National Library of Medicine (US). 2000- [cited 2014 Aug 17]. Available from: http://clinicaltrials.gov/show/NCT02139371 NLM Identifier: NCT02139371

(83)   LeBeau, A. M.; Duriseti, S.; Murphy, S. T.; Pepin, F.; Hann, B.; Gray, J. W.; VanBrocklin, H. F.; Craik, C. S. *Cancer Res.* **2013**, *73*, 2070–2081.

(84)   James, M. L.; Gambhir, S. S. *Physiol. Rev.* **2012**, *92*, 897–965.

(85)   Klibanov, A. L. *Bioconjug. Chem.* **2005**, *16*, 9–17.

(86)   Tinkov, S.; Bekeredjian, R.; Winter, G.; Coester, C. *J. Pharm. Sci.* **2009**, *98*, 1935–1961.

(87)   Cordeiro, E. R.; Cathelineau, X.; Thüroff, S.; Marberger, M.; Crouzet, S.; de la Rosette, J. J. M. C. H. *BJU Int.* **2012**, *110*, 1228–1242.

(88)   Ferrara, K.; Pollard, R.; Borden, M. *Annu. Rev. Biomed. Eng.* **2007**, *9*, 415–447.

(89)   Kitzman, D. W.; Goldman, M. E.; Gillam, L. D.; Cohen, J. L.; Aurigemma, G. P.; Gottdiener, J. S. *Am. J. Cardiol.* **2000**, *86*, 669–674.

(90)   Willmann, J. K.; Cheng, Z.; Davis, C.; Lutz, A. M.; Schipper, M. L.; Nielsen, C. H.; Gambhir, S. S. *Radiology* **2008**, *249*, 212–219.

(91)   Anderson, C. R.; Hu, X.; Zhang, H.; Tlaxca, J.; Declèves, A.-E.; Houghtaling, R.; Sharma, K.; Lawrence, M.; Ferrara, K. W.; Rychak, J. J. *Invest. Radiol.* **2011**, *46*, 215–224.

(92)   Jewett, J. C.; Bertozzi, C. R. *Chem. Soc. Rev.* **2010**, *39*, 1272–1279.

(93)   Rossin, R.; Verkerk, P. R.; van den Bosch, S. M.; Vulders, R. C. M.; Verel, I.; Lub, J.; Robillard, M. S. *Angew. Chem. Int. Ed. Engl.* **2010**, *49*, 3375–3378.

(94)   Versteegen, R. M.; Rossin, R.; ten Hoeve, W.; Janssen, H. M.; Robillard, M. S. *Angew. Chem. Int. Ed. Engl.* **2013**, *52*, 14112–14116.

(95)   Zlitni, A.; Janzen, N.; Foster, F. S.; Valliant, J. F. *Angew. Chem. Int. Ed. Engl.* **2014**, *53*, 6459–6463.

(96)   Lewis, J. K.; Wei, J.; Siuzdak, G. Matrix-assisted Laser Desorption / Ionization Mass Spectrometry in Peptide and Protein Analysis. *Encyclopedia of Analytical Chemistry*, **2000**, 5880–5894.

(97)   Marschall, C.; Lengyel, E.; Nobutoh, T.; Braungart, E.; Douwes, K.; Simon, a; Magdolen, V.; Reuning, U.; Degitz, K. *J. Invest. Dermatol.* **1999**, *113*, 69–76.

(98)   Hernot, S.; Klibanov, A. L. *Adv. Drug Deliv. Rev.* **2008**, *60*, 1153–1166.